Optimization of cellulose nanocrystal (CNC) concentration in polycaprolactone bio-composites for bio-plotting: a robust interpretation of the reinforcement mechanisms

Nectarios Vidakis · Markos Petousis · Nikolaos Michailidis ·
Constantine David · Nikolaos Mountakis · Vassilis Papadakis ·
Evangelos Sfakiotakis · Dimitrios Sagris · Apostolos Argyros

Abstract Bioabsorbable and biodegradable composites have experienced rapid growth, owing to their high demand in the biomedical sector. Polymer-cellulose nanocrystal (CNC) compounds were developed using a medical-grade poly (ε-caprolactone) (PCL) matrix to improve the stiffness and load-bearing capacity of pure PCL. Five PCL/CNCs filament grades were melt-extruded, pelletized, and fed into an industrial bioplotter to fabricate specimens. To assess the effects of CNCs on pure PCL, 14 tests were conducted, including rheological, thermomechanical, and in situ micro-mechanical testing, among others. The porosity and dimensional accuracy of the samples were also documented using micro-computed tomography while scanning electron microscopy was employed for morphological characterization. Overall, the 4.0 wt % CNCs loading accomplished the optimum mechanical response, with an increase in its tensile (19.1%) and flexural strength (12.6%) compared to pure PCL. Concurrently, this grade exhibited the highest MFR, minimum porosity, and highest nominal-to-actual geometric accuracy, thereby convincingly interpreting the reinforcement mechanisms.

N. Vidakis (✉) · M. Petousis · N. Mountakis ·
E. Sfakiotakis
Department of Mechanical Engineering, Hellenic
Mediterranean University, 71410 Heraklion, Greece
e-mail: vidakis@hmu.gr

M. Petousis
e-mail: markospetousis@hmu.gr

N. Mountakis
e-mail: mountakis@hmu.gr

E. Sfakiotakis
e-mail: esfakiotakis@hmu.gr

N. Michailidis · A. Argyros
Physical Metallurgy Laboratory, Mechanical Engineering
Department School of Engineering, Aristotle University
of Thessaloniki, 54124 Thessaloniki, Greece
e-mail: nmichail@auth.gr

A. Argyros
e-mail: aargyros@auth.gr

C. David · D. Sagris
Department of Mechanical Engineering, International
Hellenic University, 62124 Serres Campus, Greece
e-mail: david@ihu.gr

D. Sagris
e-mail: dsagris@ihu.gr

V. Papadakis
Department of Industrial Design and Production
Engineering, University of West Attica, 122 43 Athens,
Greece
e-mail: v.papadakis@uniwa.gr

Introduction

The development of high-performance multifunctional materials tailored for specific applications is a key requirement for Additive Manufacturing (AM). To achieve this, nanofillers have been combined with polymeric matrices to enhance their mechanical strength (Vidakis et al. 2022c). Moreover, various composites that demonstrate properties suitable for fields, such as medicine, have been introduced. For instance, antibacterial properties have been induced in polymeric materials in vat photopolymerization (VPP) (Vidakis et al. 2023g) and Material Extrusion (MEX) AM technology (Vidakis et al. 2023d, 2023h, 2023e). Sustainable green materials are also popular in 3D printing (Vidakis et al. 2023a), especially in biomedical applications (Arif et al. 2023), whereas soft materials have recently attracted the attention of the scientific community (Tariq et al. 2023). The broad use of 3D printing in healthcare and medical applications has often been reported in the literature (Kholgh Eshkalak et al. 2020).

A relatively new yet rapidly implemented 3D printing technology with significant potential in tissue engineering and biomimetics is bio-plotting, owing to its capacity to address several engineering challenges encountered in the biomedical industry. Therefore, they have attracted considerable research interest in recent years (Jian et al. 2018). The use of 3D bioplotting technologies also reflects the growing demand for the controlled assembly of biologically appropriate materials (Mironov et al. 2006). The development of tissue and biodegradable scaffolds is frequently stimulated by biomolecules such as growth factors (Giraud et al. 2012). Although traditional tissue engineering methods have demonstrated clinical success in the construction of a variety of tissues (Place et al. 2009), difficulties persist in the construction of complex tissues and organs. Some examples include the lack of readily available biomaterials for tissue assembly, inadequate scaffold production techniques that might imitate tissue microarchitecture, and approaches to distributing various cell types to

the correct spots within the bio-scaffold (Billiet et al. 2012). Several criteria, including biodegradability, biocompatibility, structural capacity, geometrical conformity, and moderate porosity must be addressed to create optimal scaffolds for tissue regeneration (Seol et al. 2012). Particle leaching (Prasad et al. 2017), solvent casting (Nonato et al. 2019), and freeze-drying (Grenier et al. 2019) are some of the methods employed to fabricate scaffolds for tissue engineering applications. Although these approaches can create structures that are required, it is still challenging to manage the size, microarchitecture, and interconnectedness of pores that carry nutrients and oxygen that cells need to survive (Seol et al. 2014). Additionally, scaffolds may still include organic solvents that are used to dissolve biomaterials, and their lingering residues could be hazardous to cells (Peltola et al. 2008).

Poly (ε-caprolactone) (PCL) is a biocompatible and bioabsorbable polymer that has been extensively studied owing to its unusual physicochemical properties (Scaffaro et al. 2017). PCL is a biodegradable polymer widely used in biomedical applications (Scaffaro et al. 2016a), for the expansion of bioprocesses (Scaffaro et al. 2016b), and in tissue engineering, mainly as a matrix material in composites (Arif et al. 2022). The applicability of PCL in hard-tissue repair is restricted by the high elongation at break and relatively low elastic modulus of ductile polymers (Hutmacher 2000). All of these factors have led to numerous scientific studies that have focused on the creation of high-performance electrospun PCL scaffolds, such as biopolymer blends (Bauer et al. 2016), and the utility of nanofillers (Ghorbani et al. 2015). More specifically, scientific literature describes a variety of nanofillers, such as biopolymeric nanoparticles (Zhu et al. 2015) and multi-walled carbon nanotubes (Liao et al. 2012), which are employed to enhance the biomechanical response of PCL. Currently, graphene and its derivatives are the most effective additives for developing high-performance materials (Zhang et al. 2016). Another study examined the mechanical characteristics of nanocomposites composed of PCL homopolymers with nanofibrillated bacterial cellulose (NFBC). The most rigid film that had the greatest Young's modulus and optimum strength, measuring 57.3 and 661.3 MPa, respectively, was made by the nanocomposite containing 13 wt % cellulose. These findings indicate that NFBC is a superior reinforcement material (Hashim et al. 2022a). Epoxy glass

composites have been introduced into PCL to develop self-healing composites (Simonini et al. 2023). Cellulose has been employed to reinforce PCL for the development of composites in the form of nanofibers (Lee et al. 2011) and nanofibrillated bacterial cellulose (Hashim et al. 2022b).

Cellulose, the most prevalent biopolymer derived from plants or microbes, has been extensively employed in the production of green products (Qiu et al. 2018). Several nanosized cellulose particles (Khalid et al. 2021), such as cellulose nanofibers, nanofibrillated cellulose, and cellulose nanocrystal (CNC), can be produced using a variety of mechanical and chemical processes (Moon et al. 2011). Because of the ester sulfate groups added by acid hydrolysis, cellulose can be stably distributed in water in colloidal suspensions, exhibiting good hydrophilicity (Yu et al. 2019). Cellulose has been used in the development of films with dielectric nanocomposites (Zhang et al. 2023), natural rubber composites (Noguchi et al. 2023), and composites with complex geometries (Baranov et al. 2023). CNCs have attracted considerable interest as bio-based strengthening nanomaterials for polymeric compounds (Khalid et al. 2023) owing to their desirable physical and chemical characteristics, such as their low density ($1.6–3$ g/cm^3) (Mujtaba et al. 2017), superior tensile strength ($7.50–8.50$ GPa) (Grishkewich et al. 2017), high crystallinity (Gong et al. 2017), high elastic modulus (approximately 140.0 GPa) (Grishkewich et al. 2017), and hydroxyl-rich surface (Lam et al. 2012). In an attempt to replace non-biodegradable plastics, researchers have proposed the concept of bio-nano compounds made of biodegradable PCL and regenerated CNCs crosslinked with peroxide. Heat shrinkage of the composites occurs by the irrevocable entrapment of CNCs in the 3D percolating network, suggesting a potential for heat-triggered shape memory in reacting bionanocomposites (Avella et al. 2022). Cellulose has been incorporated into various types of additive manufacturing (AM) technologies for 3D printing, serving as a reinforcing agent in the form of nanofibers within the matrices. These nanocomposites have been widely used in the medical field. For instance, in VPP 3D printing, nanocomposites have been developed using biomedical-grade resins (Vidakis et al. 2022a, 2023b). Additionally, cellulose nanofibers (CNFs) have been combined with other additives to impart multifunctional properties

to nanocomposites (Vidakis et al. 2022b). Similarly, in MEX 3D printing, cellulose has been introduced into various matrices including polycarbonate (PC) (Vidakis et al. 2021), Polylactic Acid (PLA) (Petousis et al. 2022), and polyamide 12 (PA12) (Vidakis et al. 2023f). CNCs are popular in AM and are primarily used in biomedical applications (Du et al. 2019; Khalid et al. 2023). They have been used in hydrogels (Wang et al. 2018; Du et al. 2019; Ma et al. 2021; He and Lu 2023) and inks (Hausmann et al. 2018)for the development of scaffolds (Li et al. 2019a), often in VPP 3D printing (Palaganas et al. 2017; Li et al. 2019b). However, their use in MEX 3D printing is limited.

Through fourteen tests, including in-situ micro-tensile testing, micro-computed tomography (μ-CT) for determining the 3D printing structural porosity, and the nominal to actual dimensional accuracy of the 3D printed samples manufactured with the bio-composites developed, this investigation aims to examine in depth the effects of adding CNCs particles on the thermomechanical and rheological characteristics of a medical-grade PCL polymer. Both the matrix and the filler are biocompatible and medical-grade materials. The research objective was to mechanically upgrade the PCL polymer to a form compatible with bioplotting 3D printing that can be directly exploited in medical applications, such as scaffolds, for example, using biocompatible materials. PCL is a soft material, but it is still popular in biomedical applications such as scaffolds. Therefore, improving mechanical performance is advantageous and can further expand its usability. The nanocomposites were prepared using a thermomechanical extrusion method in the filament form. They were then pelletized to produce the raw nanocomposite material for the bioplotting process, with which the samples for mechanical testing and the remaining tests conducted within the context of the research were manufactured.

Experiments on the manufactured specimens were conducted according to the American Society for Testing and Materials (ASTM) standards. The thermal stability of the bio-compounds was examined using Thermogravimetric Analysis (TGA) and Differential Scanning Calorimetry (DSC). Energy Dispersive Spectroscopy (EDS) and Raman spectroscopy were used to study the elemental and chemical structures of the grades used or developed. The surface microstructures of various 3D bioprinted

objects (tensile, flexural, and μ-CT scan specimens) and filaments were investigated using Atomic Force Microscopy (AFM) and field-emission scanning electron microscopy (feSEM) to ascertain the impact of CNCs concentration on the morphological characteristics of the samples. A solid interpretation of the reinforcing mechanisms is required. The PCL/CNCs bio-composites with 4-weight percent loading demonstrated a high improvement in all tests. At the same time, this grade expressed the lowest nominal to actual dimensional deviation, lowest porosity, and highest melt flow-rate (MFR) index. These findings reveal the capability of PCL/CNCs biocompounds for 3D bioplotting by extending the range of potential biomedical applications and satisfying the need for biodegradable and biocompatible materials with enhanced mechanical properties. 3D bioprinting is a method used to build other living cells, drug particles, and medical-related structures (Ozbolat et al. 2016; Kačarević et al. 2018). The bioplotting method was used herein to 3D print parts using biocompatible materials. These materials were tested for their performance and ready for use in scaffolds and other bio-related applications. The parts were built in a clean room in an infrastructure ready for 3D printing of living cells, following the same procedure.

Materials and methods

Figure 1 demonstrates the approach followed herein. The left part shows the steps of the procedure implemented to prepare, test, and evaluate the specimens developed in this study. Furthermore, relevant photographs for each phase of the experimental course are shown on the right side of Fig. 1.

Materials

Medical-grade PCL, produced following EN ISO 13485 and purchased from ITV Denkendorf Produktservice GmbH in Germany, was used in the investigation. It is a homopolymer of PCL. PCL has a melting point of 57.5 ± 2.5 °C, purity > 99.0%, and an intrinsic viscosity of 1.9 to 0.3 dl/g, according to the manufacturer's specifications. Nanografi Nanotechnology (Ankara, Turkey) supplied CNCs in white spray-dried powder (6.0% moisture, 10–20 nm), with a decomposition temperature of 349 °C and a density of 1.49 g/cm^3. This filler was employed to enhance the PCL matrix characteristics and overall quality of the compounds.
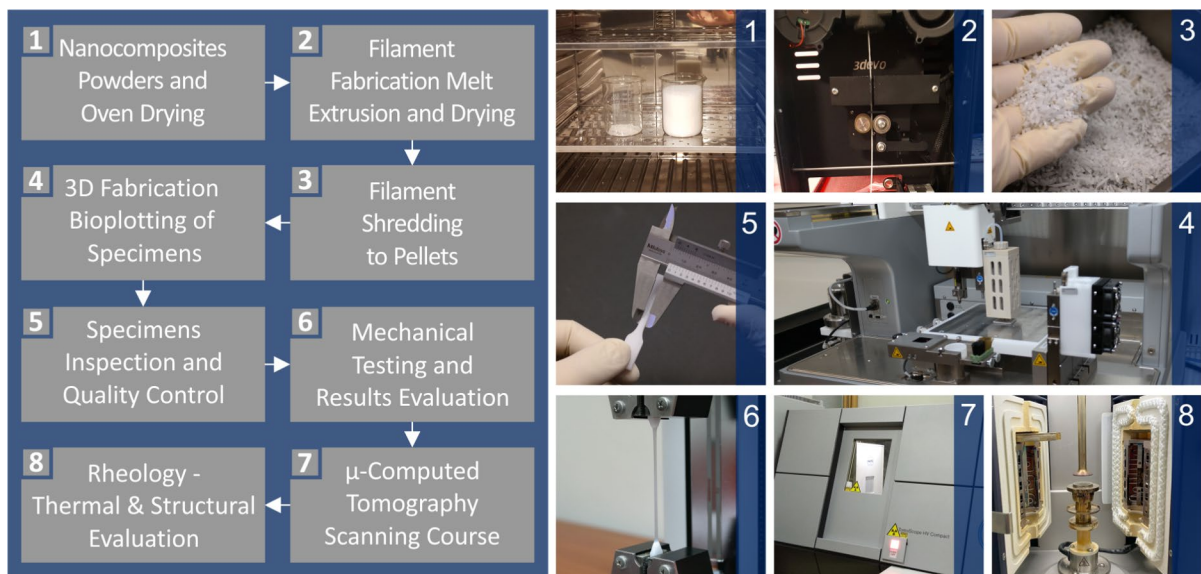
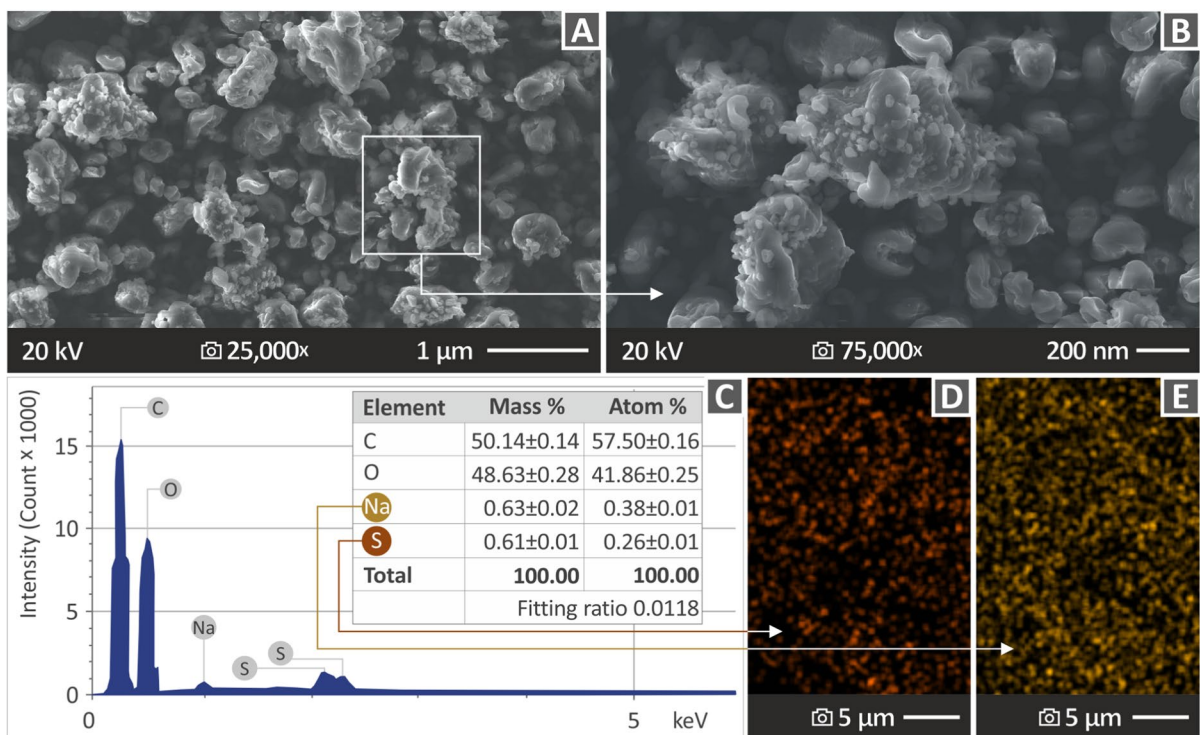**Fig. 1** Flowchart of the research procedure implemented with appropriate images for each phase

Filament fabrication (extrusion and drying)

Before producing the compounds, the CNCs powder was analyzed using a specialized feSEM, the JSM/IT700HR (Jeol Ltd/Tokyo/Japan). Figure 2 shows the results of the Energy Dispersive X-ray Spectroscopy (EDS) analysis used to identify the chemical components of the CNCs. SEM micrographs (Fig. 2B) Investigated their microstructurescture. The nanoscale size of the particles was verified using SEM. Their shapes are also in agreement with those in the literature (El-hadi 2017).

Figure 2D illustrates the presence of carbon (C), indicated by the higher peak in the EDS analysis graph. Additionally, oxygen was found to constitute up to 48.63% of the mass, which was expected given that hydroxyl (OH) groups (both secondary and primary) are the major chemical groups found on cellulose materials, including specific CNCs, as stated in the manufacturer's datasheet. Although oxygen is a component of the hydroxyl groups (OH), which are not specifically mentioned in the datasheet, it can be assumed that oxygen is present in the CNCs powder in the form of these hydroxyl groups. Furthermore, trace levels of Na (approximately 0.63% of the mass) and S (approximately 0.61% of the mass) were identified, which is consistent with the CNCs manufacturer, claiming that it contains sulfate (half-ester) groups added during the acid hydrolysis process. This indicates that the CNCs powder contained both sulfur (S) and sodium (Na). Figure 2E and F show the presence of Na and S, respectively.

The pure materials were dried for 24 h at 50 °C to remove any remaining moisture. Five different material combinations, including pure PCL, were created by varying the weight percentage (wt %) of CNCs with concentrations of 2.0, 4.0, 6.0, and 8.0 wt %. Hence, the PCL compounds consisted of CNCs particles and the residual weight percentage was pure PCL. Under ambient conditions (23 °C) and 4000 rpm, a high-wattage mixer was used for 30 min to blend the CNCs powder with PCL. After blending, the mixtures were dried a second time. The filaments were produced using a 3Devo/Composer melt

Element	Mass %	Atom %
C	50.14±0.14	57.50±0.16
O	48.63±0.28	41.86±0.25
Na	0.63±0.02	0.38±0.01
S	0.61±0.01	0.26±0.01
Total	**100.00**	**100.00**
	Fitting ratio 0.0118	

Fig. 2 Evaluation of CNCs **A** SEM micrograph at 25,000×, **B** SEM micrograph at 75,000×, **C** EDS graph and elemental analysis, **D** EDS mapping of elemental sulfur, and **E** EDS mapping of sodium

extrusion device (3Devo B. V/Utrecht/Netherlands) fitted with a feedback feature to ensure diametric conformity. Subsequently, the filaments were pelletized using a 3Devo/Shredder by 3devo B.V. The industrial dual (cold and hot) headed 3D Bioplotter from EnvisionTEC (Dearborn/Michigan/United States) was then fed with nanocomposite pellets to fabricate standard samples for mechanical testing. Before shredding, the filaments were subjected to various tests to assess their diameters, tensile strengths, moduli of elasticity, and other structural characteristics. The results of these tests are provided in the supplementary material accompanying this research study.

3D printing of the specimens (Production of 3D bio-printed samples using a 3D Bio-plotter, samples for mechanical testing, and microcomputed tomography).

To manufacture samples made of PCL/CNCs composites, pellets from the shredded filaments were pelletized and fed into a 3D Bio-plotter (EnvisionTEC, Michigan, United States). The nominal geometry of the specimens, created in STL format using Computer-Aided Design (CAD) software, was sliced into layers compatible with the 3D Bioplotter using the Perfactory RP program, each with a predetermined thickness. The Visual Machines software tool was used to configure the plotter settings, including the speed and air pressure. The specimens were fabricated according to the tensile test standard ASTM-D638 and the flexural test standard ASTM-D790. Additionally, μ-CT scan specimens were created for μ-CT analysis. Figure 3 illustrates the set of defined parameters utilized for the 3D bioplotting process, as well as the full-dimensional features of the test specimens. The 3D printing parameters were defined based on preliminary tests and by consulting relevant literature (Vidakis et al. 2023c).

Raman spectroscopy

A HORIBA Scientific LabRAM HR Raman Spectrometer (Kyoto, Japan) was used to conduct Raman spectroscopy. The lateral and axial resolutions of the microscope were measured at 1.7 and 2 μm, respectively. Three successive optical windows were required to capture the spectrum, ranging from 50 to 3900 cm^{-1}. Each point had a 10 s exposure time and five accumulations.

The system meets the following requirements: Olympus objective lens (LMPlanFL N) with a numerical aperture of 0.5, 50×exaggeration, and a 10.60 mm functioning operational distance; a 600-groove grating producing a Raman spectrum resolution of approximately 2 cm^{-1}; and a Neutral Density filter regulating the laser power to 4 mW on the samples with a 10% transmittance. For excitation, the highest output power of the 532 nm solid-state laser module was 90 mW.

TGA, DSC, and rheometric analysis

The ability of the bio-compounds to sustain their structural integrity at elevated temperatures was evaluated using TGA. Experiments were performed using a PerkinElmer Diamond apparatus (PerkinElmer Inc., Waltham, MA, USA) in an inert nitrogen environment. Starting at room temperature and increasing to 550 °C throughout the experiments, the temperature was steadily increased by 10 °C per minute. DSC was used to examine the thermal response of the nanocomposites. TA-Instruments/Discovery-Series DSC 25 (TA Instruments/Delaware/United States) was used for this purpose, featuring a cycle ranging from 25 to 300 °C and then down to 25 °C with a step span of 15 °C per minute.

Two parallel plates, along with the environmental conditions chamber to control the temperature, were added to a DHR/20 (Discovery-Hybrid-Rotational-Rheometer, also by TA Instruments) to evaluate the rheological features of the nanocomposites. The diameter of the parallel plates used in the experiments was 25 mm and the geometric gap between the plates used during the rheometry experiments was 1 mm. To avoid overheating and failure, 10 s of data were recorded for each measurement point. Rotational rheometry experiments and Melt Flow Rate (MFR) measurements were combined to assess the flow characteristics of the biocomposites via a hole with a predefined diameter and length under certain pressure and temperature conditions. The MFR measurements were performed according to ASTM D1238-13, the international standard for MFR testing.
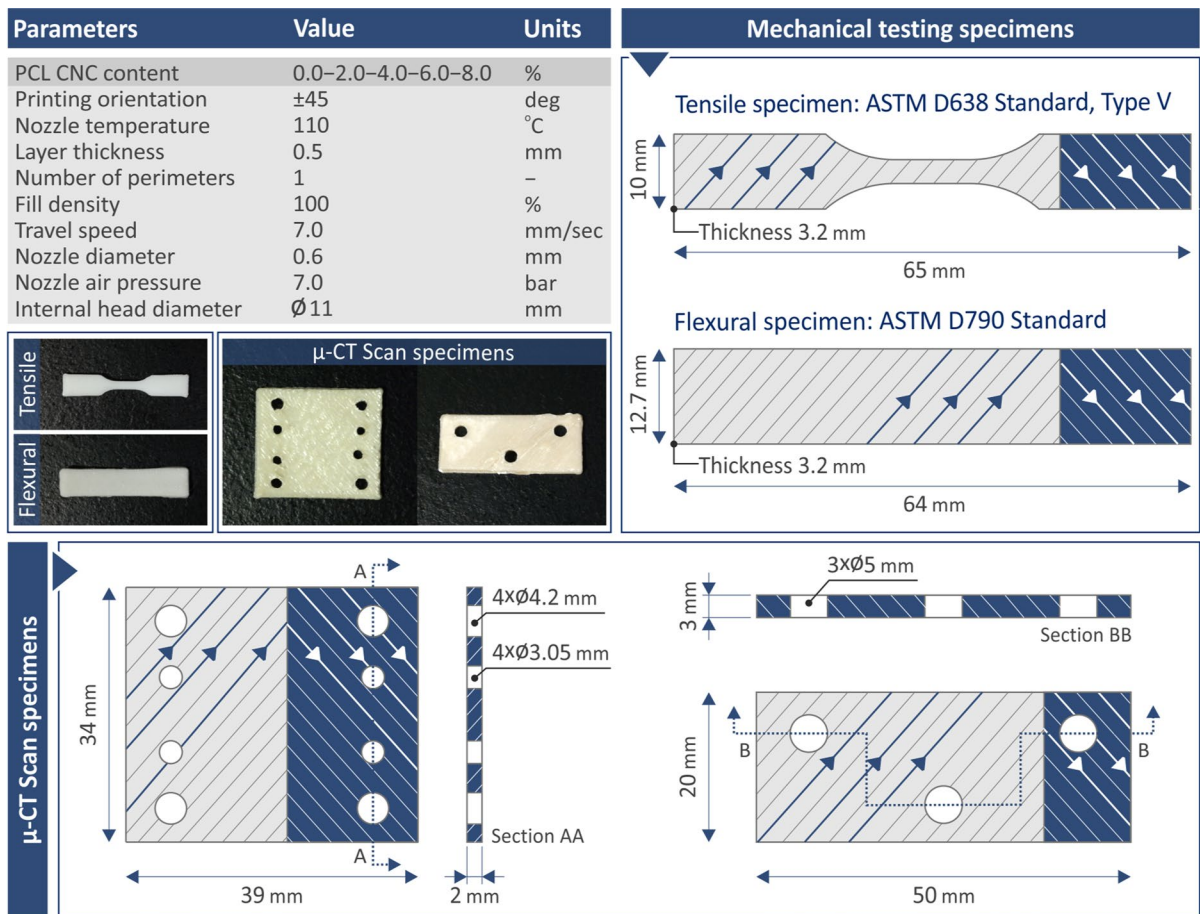
Fig. 3 The 3D bioplotting parameters were used to fabricate the test specimens, as well as the ASTM specifications with the dimensions of the specimens for each mechanical test

Mechanical testing of the 3D printing of the specimens (tensile and flexural tests)

To assess the mechanical capacity of the 3D bioplotted materials under external stress conditions, tests were performed according to the specific ASTM standards. The main objective of the mechanical tests was to document the stiffness, strength, and toughness in the uniaxial and bending loading states. Additionally, it was of interest to determine how CNCs nanoparticle loading affects the mechanical response of the nanocomposites, along with determining the optimum filler percentage. All the tests were conducted under normal ambient conditions of 23 °C and an average humidity of 55%. Five samples of each composite grade were prepared and analyzed. An Imada/MX2 apparatus (Imada Inc/Northbrook/USA) with a 10.0 mm per min strain rate and ordinary grips was used to conduct the tensile tests. Three-point bending (flexural) tests were performed using Imada MX2 equipment with a 10.0 mm/min strain rate and a specimen support span of 52.0 mm.

In situ *SEM micro tensile tests*

A scanning electron microscope (In Touch Scope JSM-IT510, Jeol/Tokyo/Japan) was used to conduct in situ micro-tensile testing of specimens made of pure PCL to study the failure mechanisms of the samples. Prior to SEM examination, a sputter coater (SC7620, Quorum Technologies Ltd., UK) was used to prepare the specimens. A Pd disc target was placed on the magnetron sputtering head. By regulating the vacuum chamber pressure to 6×10^{-2} mbar, a

plasma current of 20 mA, and an argon gas pressure of 0.5 bar, the sputtering process was carried out for 90 s.

Utilizing an in situ SEM tensile stage (MT5000, with a 5 kN loadcell capacity, Deben Ltd. UK), the specimens were subjected to microtensile testing. To this end, the specimens were clamped longitudinally between two jaws. The sample was kept in the center of the field of view and subjected to a tensile load by a microthreaded lead screw driving the jaws coaxially in opposing directions. The travel distance was 5.50 mm, and the strain rate was 0.50 mm/min. Specific software was used to adjust the setup parameters and feed the stress/strain data into the computer. In situ micro-tensile testing enables dynamic microstructural studies within the SEM, while the samples are subjected to tensile stress, offering insightful information on material performance.

To characterize the microstructures of the lateral and fractured surfaces of the 3D bio-printed specimens fabricated for mechanical testing, they were comprehensively analyzed using another field emission scanning electron microscope (JSM-IT700HR/ Jeol Ltd/Tokyo/Japan) in the high vacuum mode at 20.0 kV. SEM was used to capture the micrographs of these specimens at various magnifications after they were appropriately gold-sputtered.

Micro computed tomography (μ-CT) investigations

By means of 3D Computed Tomography (CT), the structural inspection of the 3D bio-printed samples was accomplished. A μCT apparatus (Tomoscope HV Compact/Werth-Messtechnik GmbH, Germany) was used for this purpose. Micro-computed tomography was used to quantify the quality indicators of the 3D-printed workpieces, such as porosity and dimensional accuracy, to study and identify possible correlations between these findings and the mechanical test results.

Results

Raman spectroscopy analysis

Distinct Raman spectra of PCL and PCL/CNCs for each grade are shown in Fig. 4A. Figure 4B shows the variations that were observed as a result of the incorporation of CNCs nanoparticles by subtracting the measured spectrum of pure PCL from each signal of the nanocomposites. The Raman peak of pure PCL is shown in Table 1 along with the corresponding peak assignments gathered from relevant literature. Table 2 shows the associated Raman peak differences between the PCL pure PCL and PCL/CNCs samples, as well as their assigned values according to the literature.

Table 3 presents the cellulose-related Raman bands studied to examine the presence of CNCs in our samples and how they are related to the percentage weight added to PCL. Some spectral changes were observed; however, these changes were not significant. Specifically, we noticed a small gradual increase in the

Fig. 4 Raman spectra from **A** PCL Pure and PCL/CNCs 2, 4, 6, and 8 wt%, and **B** PCL Pure, PCL/CNCs 2, 4, 6, and 8 wt%, when PCL Pure is subtracted
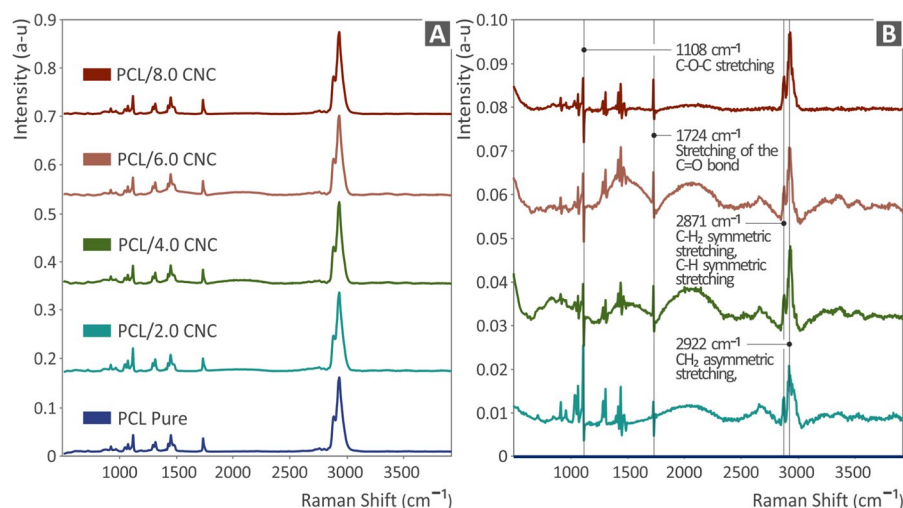
Table 1 Main Raman peaks of raw PCL identified and their assigned assignments

Wavenumber (cm^{-1})	(Raman) peaks association with bonds
870	C–COO/stretching (Lin et al. 2021)
915	In-plane bending of CH$_2$ (Camerlingo et al. 2007)
1040	C–CH$_3$ / stretching (Lin et al. 2021)
1065	C–O –C / stretching (Lin et al. 2021)
1109	C–O–C / stretching (Lin et al. 2021)
1285	C–O–C / stretching (Lin et al. 2021)
1305	Stretching of the C=O bond (Gatin et al. 2022)
1418	C–H$_3$ / deformation (Stuart 1996)
1441	C–H$_3$ / deformation (Stuart 1996) C–H$_2$ / deformation (Zimmerer et al. 2019)
1724	Stretching of the C=O bond (Luiz et al. 2007; Peris-Díaz et al. 2018; Gatin et al. 2022)
2870	C–H$_2$ / symmetric stretching (Makarem et al. 2019); C–H / symmetric stretching
2919	CH$_2$ / asymmetric stretching (Makarem et al. 2019)

Table 2 The main Raman peak differences between the pure PCL and PCL/CNCs samples are depicted and their associated assignments

Wavenumber (cm^{-1})	Change	(Raman) peaks associated with bonds
1108	Small increase	C–O–C / stretching (Lin et al. 2021)
1724	Small Increase	Stretching of the C=O bond (Luiz et al. 2007; Peris-Díaz et al. 2018; Gatin et al. 2022)
2871	Increase	C–H$_2$ / symmetric stretching (Makarem et al. 2019); C–H / symmetric stretching (Liu et al. 2006)
2922	Increase	CH$_2$ / asymmetric stretching (Makarem et al. 2019)

Table 3 Cellulose-related Raman bands

Change	Type	Raman shifts (cm^{-1})	Assignments
Increase	Similar	2968	CH/CH$_2$ stretch modes polarized (Makarem et al. 2019)
NO		2930	CH stretching of hemicellulose (Chylińska et al. 2014)
Increase	Similar	2895	CH stretching of hemicellulose (Chylińska et al. 2014)
Increase	Similar	1470	cellulose Iβ - > CH$_2$ bending mode (shifted to 1460 cm^{-1} in spectra of other allomorphs) (Makarem et al. 2019)
NO		1374 – 1378	Cellulose (Makarem et al. 2019)
Increase	Gradual	1313	Cellulose aliphatic OH bend vibration, strong
Increase	Gradual	1121	Cellulose (Chylińska et al. 2014)
Increase	Gradual	1093	Cellulose (Chylińska et al. 2014)
NO		971	Cellulose (Chylińska et al. 2014)

cellulose Raman bands at 1093 and 1121 cm^{-1}, but these were not present in the 8 wt % CNCs.

A small gradual increase was observed in the strong band at 1313 cm^{-1}, which appeared at 1309 cm^{-1} in our measurements, most probably because of the different environmental stresses from the cell wall to our composite. The band at 1470 cm^{-1} showed a similar increase in all samples, except for the 4.0% CNCs. A similar increase was observed in all samples at 2895 and 2967 cm^{-1}.

TGA and DSC test results

The weight loss over the temperature rise is shown by the TGA plots of the raw PCL and the studied bio-composites (see Fig. 5A). As shown in Fig. 5A, the inclusion of CNCs nanoparticles did not significantly affect the capacity of the PCL material to withstand decomposition heat. The inclusion of CNCs in the PCL matrix shifted the temperature at which acute weight degradation began to lower. All the nanocomposites began to lose weight at approximately 310 °C.

It should be mentioned that the weight loss initiation temperature threshold was far higher than the temperature profiles used in melt filament extrusion and bioplotting processes, as described above. The residual weight of the TGA sample is shown in the inset of Fig. 5A. This weight is consistent with the filler content of the compound. Because the residual mass increased with increasing CNCs loading in the composites, it is safe to assume that the CNCs did not fully decompose during TGA. According to the manufacturer, the decomposition temperature of Crystalline Nanocellulose (acquired with TGA in N_2) was 349 °C, whereas the composites started to decompose at approximately 420 °C, according to the TGA graphs produced in this study. DSC heat-flow plots for the selected PCL material and bio-compound

PCL/CNCs grades are shown in Fig. 5B. As can be seen, all the material patterns were similar, and the relaxation peaks were discernible.

Rheometric analysis

Rheological measurements are shown in Fig. 6A. The viscosity and stress of the samples are shown on the logarithmic axis as functions of shear rate. All the samples showed an overall drop in viscosity as the shear rate increased, indicating a shear-thinning, non-Newtonian, or pseudoplastic tendency. PCL has a moderate shear-thinning characteristic at frequencies larger than 50 rad/s and is Newtonian over a broad frequency range (0.1 50 rad/s) (Beaugrand and Berzin 2013). All the samples displayed quasi-Newtonian behavior at modest shear rates. This indicates that the viscosity of the biocomposites remained largely consistent over a range of shear speeds. Beyond this range, the viscosity of the composites may change, deviating from strictly Newtonian behavior. The viscosities of the PCL/CNCs composites suggest that they are non-Newtonian and shear-thinning, with precise properties that depend on the shear rate and CNCs content. These results offer useful information for comprehending and modifying the flow
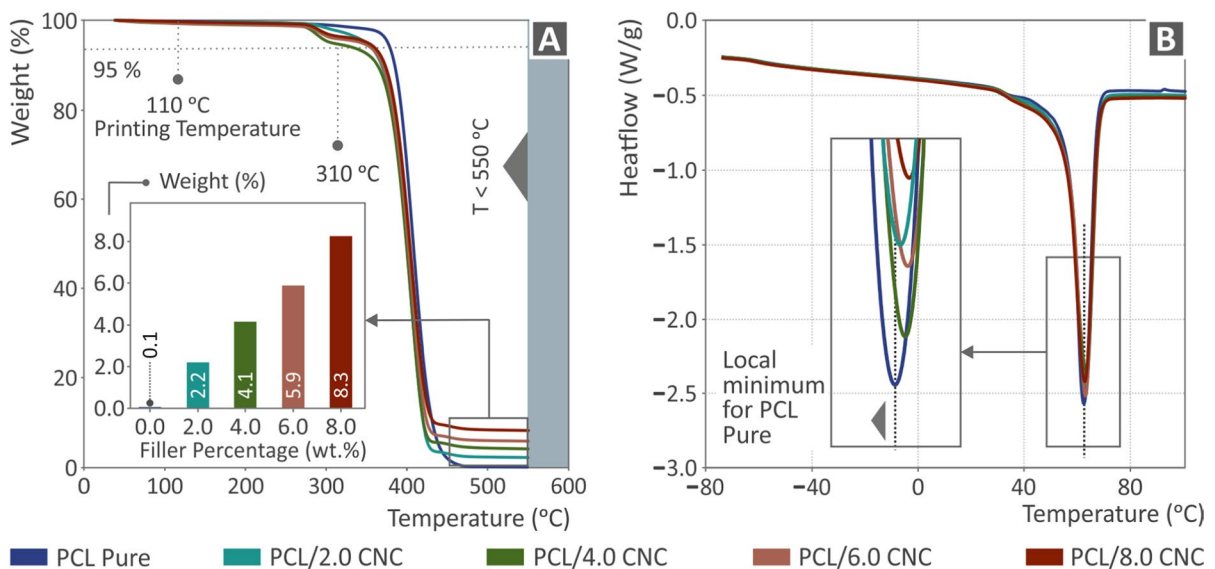
Fig. 5 Thermal assessment of raw PCL and PCL/CNCs bio-compounds using **A** thermogravimetric analysis (TGA) curves and **B** Heat-Flow Curves over temperature
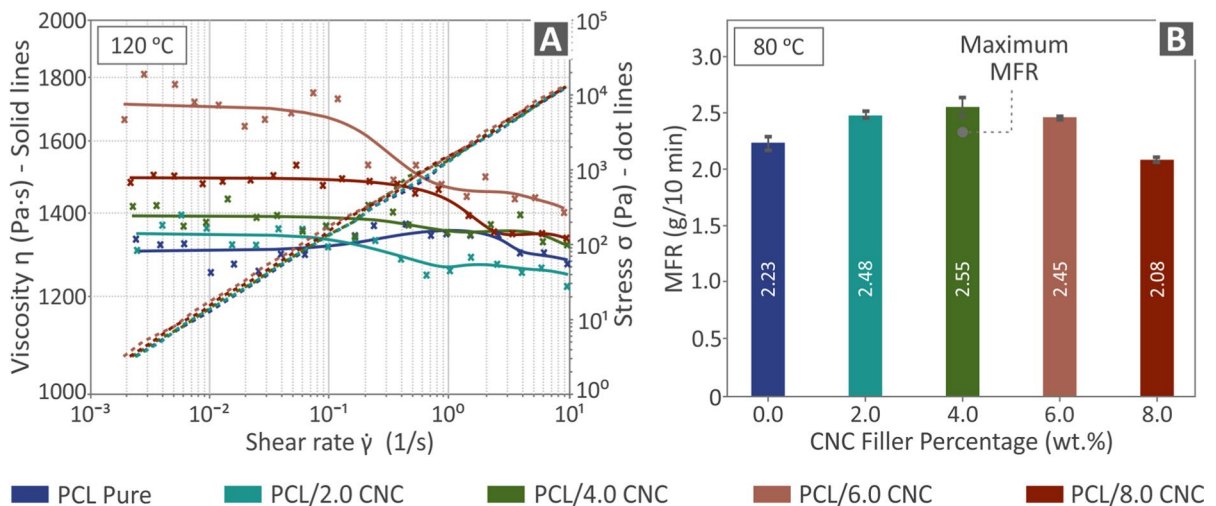
Fig. 6 Rheological analysis of PCL/CNCs bio-composites and pure PCL polymer: **a** viscosity and stress versus shear rate and **b** MFR versus filler load

characteristics of PCL/CNCs biocomposites for a variety of manufacturing applications.

Figure 6B presents the MFR (in g/10.0 min) in line with the additive weight proportion as a result of the MFR measurements. In general, the flow rate increased when fillers were added compared to that of pure PCL, reaching its maximum value at an additive loading of 4.0 wt %. Rheological measurements agreed with the observation that greater loadings appeared to gradually reduce the flow rate of the composite material with 8 wt % loading nanocomposite showing lower MFR values than the pure PCL. The viscosity of the PCL/8.0 CNCs was lower than that of the PCL/6.0 CNCs because the increase in the filler percentage in the matrix promoted interactions between the particles. Consequently, the addition of the filler to the matrix allows slippage between the PCL macromolecules, reducing the polymer chain strength and, consequently, the viscosity of the modified material.

Mechanical evaluation of 3D printed specimens

To mechanically assess the performance of the 3D Bio-printed specimens, tensile testing in line with ASTM D638-02a was carried out. Figure 7A displays a graph illustrating the relationship between strain (mm/mm) and tensile stress (MPa) for an indicative specimen (out of the five tested) of each nanocomposite material and pure PCL. The graphs are depicted up to one strain, since after the point, no valuable information is presented in the graph, and the authors wanted to present the graphs with higher resolution at the beginning of the curves.

Figure 7B shows a plot of the ultimate tensile strength (MPa) for all materials in combination with the filler percentage. Figure 7C shows the tensile modulus of elasticity (in MPa) for each additive percentage considered and pure PCL. The results of the experiment demonstrated that all the specimens with different filler concentrations exhibited superior tensile performance compared to that of the unfilled PCL polymer. With enhancements of 15.6% in stiffness and 19.1% in tensile strength, the sample with 4.0 wt % CNCs showed the most noticeable improvement. Further increase in the CNCs concentration led to no noticeable improvement in the mechanical performance. A decrease in the mechanical performance of the nanocomposites at loadings greater than 4 wt % is an indication that the saturation of the filler in the matrix begins. This was further verified by the fact that this decrease became more intense with a further increase in the filler concentration in the matrix. The saturation of the filler in the matrix negatively affects the mechanical performance of composites (Mazzanti et al. 2019).

A summary of the flexural properties of the specimens fabricated from the PCL/CNCs
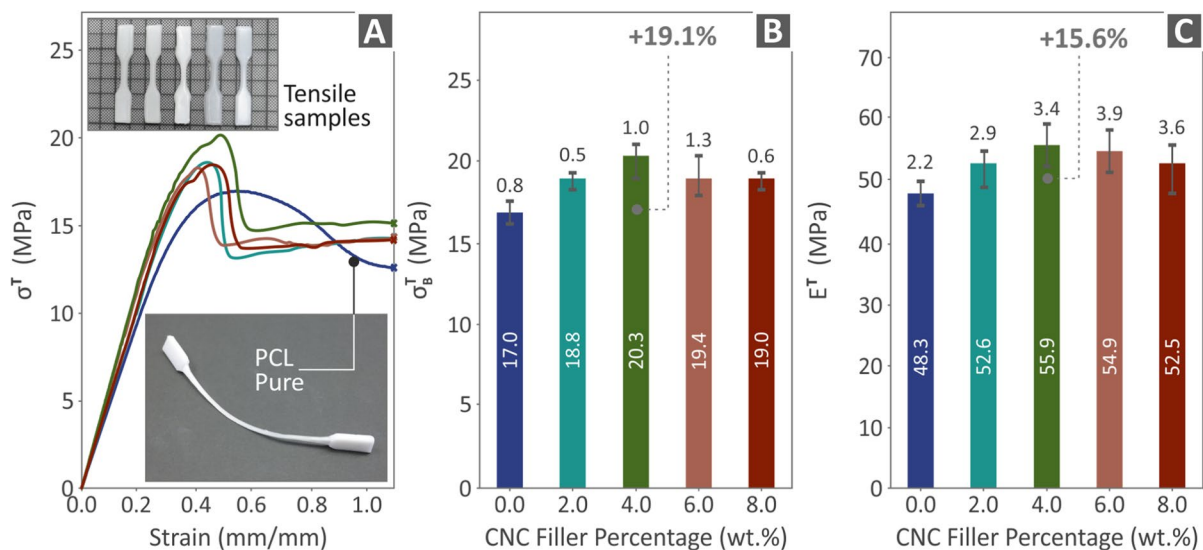
Fig. 7 The results of the tensile testing of the 3D bio-printed specimens: An indicative example of a 3D bio-printed specimen from each bio-composite material is shown in **A** representative charts presenting the relationship between tensile stress and strain, **B** average calculated values of ultimate tensile strength, and **C** average calculated values of the tensile modulus of elasticity

biocomposites and pure PCL is shown in Fig. 8. The flexural stress–strain plots for the various 3D bio-printed compounds are shown in Fig. 8A. Parts B and C of the figure show the flexural trial mean flexural strength and elastic modulus, respectively. The ASTM D790-10 standard was used to determine
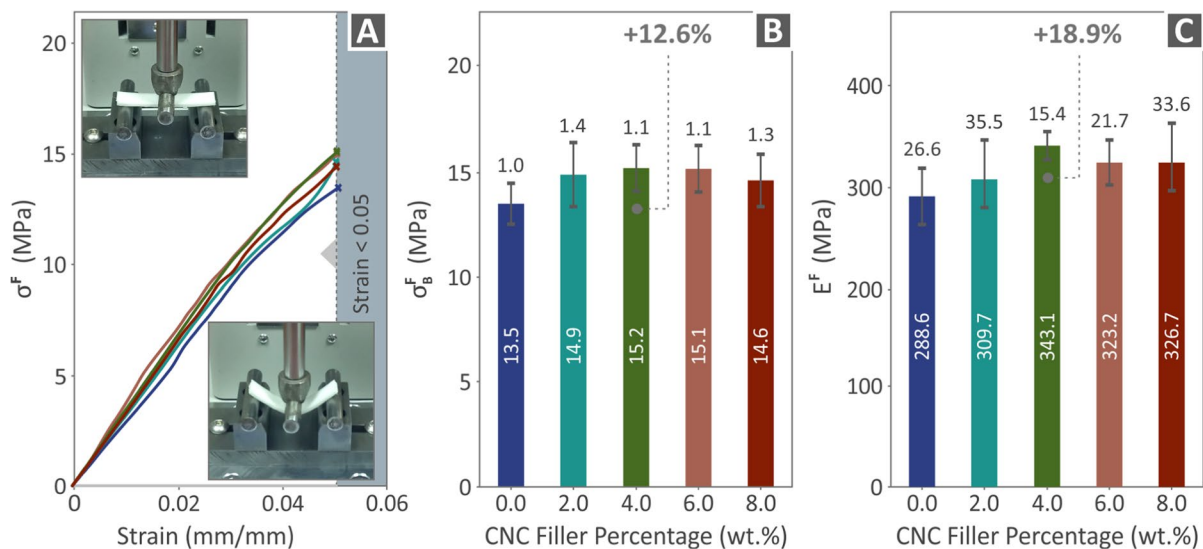
Fig. 8 Flexural test results were obtained for all specimens created using the 3D bioprinting technology. One randomly chosen sample from each biocomposite was used to analyze the stress–strain curves of various specimens for flexural strength. The results are shown in **A** stress–strain curves, **B** average calculated results and deviations for flexural strength, and **C** average results and deviations for the flexural modulus of elasticity

the average flexural strength values, which were computed at an ultimate strain of 5% according to standard instructions. The 4.0 wt % nanocomposite reached a maximum flexural strength of 15.2 MPa, indicating an increase of 12.6% compared to pure PCL. The nanocomposites loaded with 4.0 wt % also exhibited the highest flexural modulus of elasticity, amounting to 343.1 MPa, with an increase of 18.9% above the pure PCL material.

Figure 9 provides information on the toughness values (amount of energy the materials absorbed during testing determined by integrating the relevant stress–strain curve) (MJ/m^3) for the fabricated materials in the specimen and filament forms. By comprehending how a material breaks, it is possible to use the toughness ratings of the materials to acquire a safe failure strategy for several applications. As shown in Fig. 9A and B, which show the results of specimen testing, all biocomposites had greater flexural and tensile toughness values than the pure PCL polymer. In particular, the PCL/CNCs 4.0 wt % bio-composite shows a substantial improvement of 22.0 and 25.5% in tensile and flexural toughness, respectively. Additionally, Fig. 9C, which depicts the results of filament testing, shows that all composites exhibit improved toughness values, with the 4.0 wt % CNCs bio-composite showing the highest response with a 31.6% improvement over pure CNCs.

SEM morphological analysis of 3D bio-printed specimens

The fractured and side surfaces of the 3D bio-printed flexural test samples were carefully examined using SEM imaging. Two samples, pure PCL and PCL/ CNCs 4.0 wt % are displayed in Fig. 10A, and D, respectively magnified at 30×. According to the images, the connections between the layers appeared to be flawless and void-free. It is important to note that the samples lack uniform layer shapes. In Fig. 10B and C, the corresponding fractured surfaces of the specimens inspected in Fig. 10A and B are presented. Figure 10B, which depicts the pure PCL specimen at 1000×magnification, reveals a lack of smooth surfaces and discernible microcracks. The marked area in Fig. 10B is presented at a higher magnification level (5000×) in Fig. 10C. Furthermore, Fig. 10E shows that the PCL/CNCs 4 wt % specimen at 1000×magnification, reveals a smoother surface with the presence of microcracks, which are depicted in a higher magnification level of 5000×in Fig. 10F. This smoother fracture surface indicated a more brittle failure mechanism in the samples, at least at the microscale level. Images of the PCL/CNCs 8 wt % are presented in Fig. 10G, H, and I. As shown in the higher loaded samples, which had a reduced mechanical response, the 3D printing structure quality slightly worsened compared to that of the composites with lower CNCs
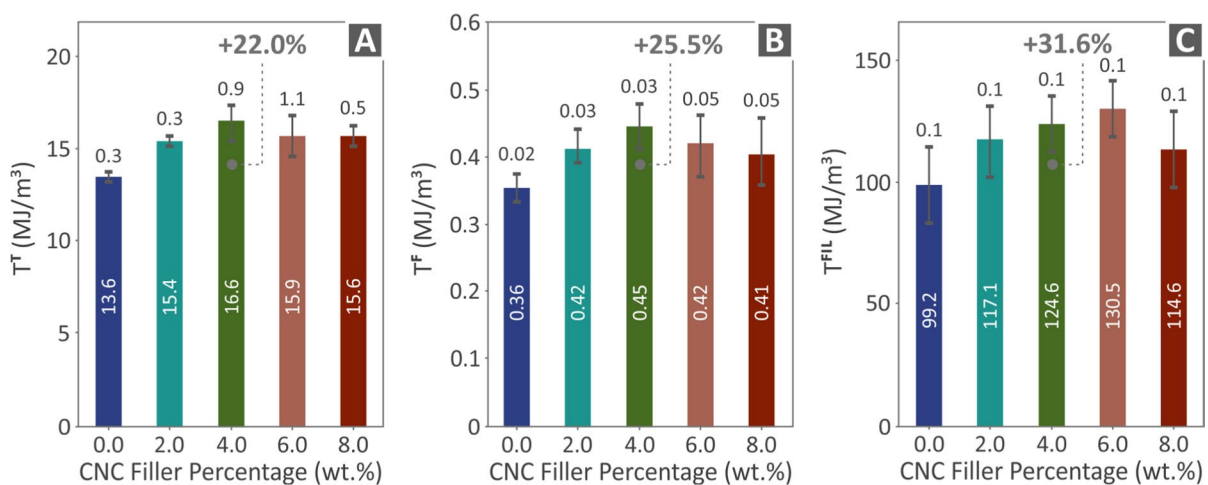
Fig. 9 Typical values and standard deviations of **A** tensile toughness of the samples, **B** flexural toughness of the samples, and **C** filament tensile toughness
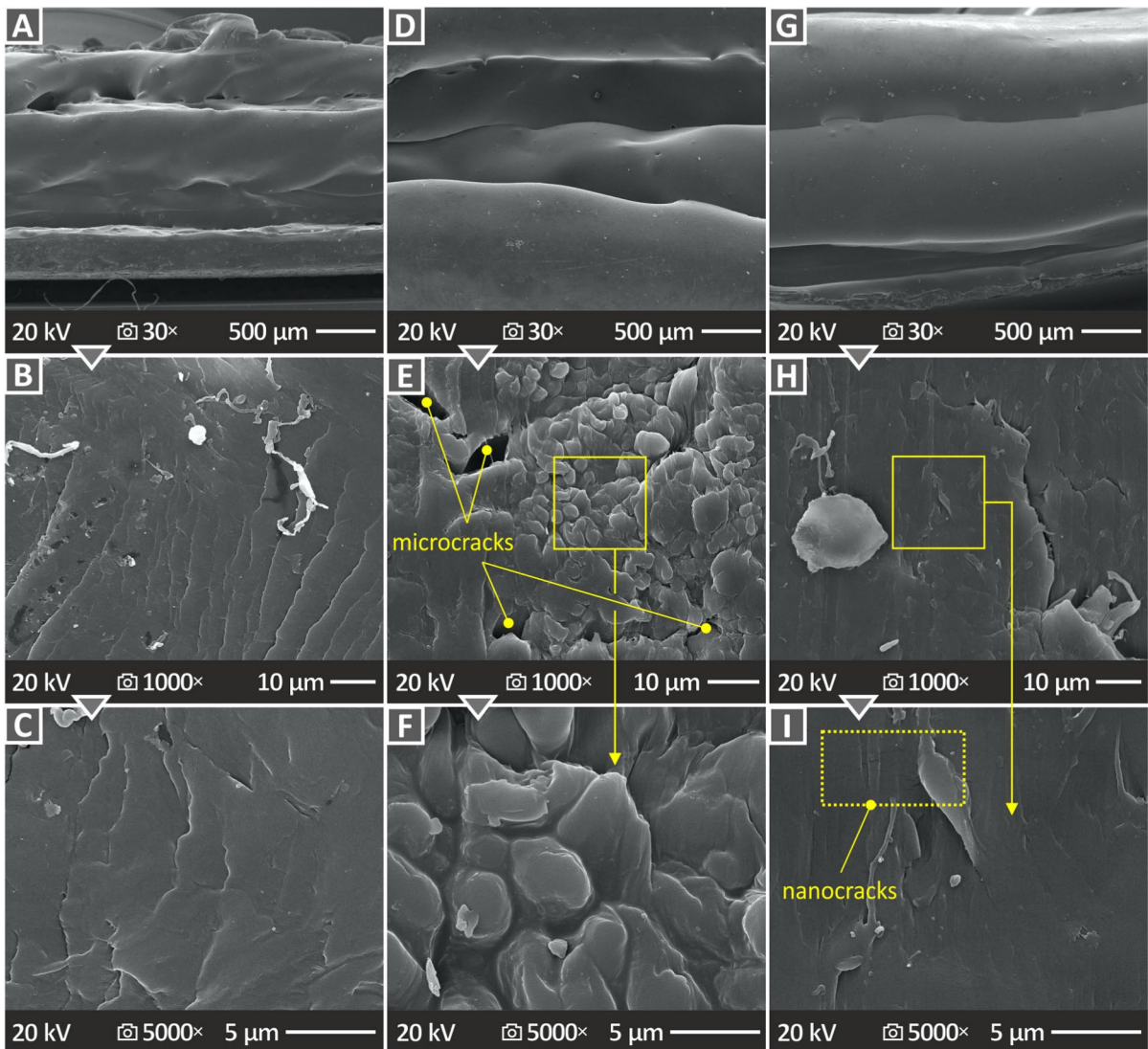
Fig. 10 SEM micrographs: **A** Lateral surface of pure PCL at 30×, **B** fractured surface depicting microcracks of pure PCL at 1000× magnification, **C** fractured surface of pure PCL at 5000×, **D** lateral surface of PCL/CNCs 4.0 wt % at 30×, **E** Fractured surface of PCL/CNCs 4.0 wt% at 1000× magnification, and **F** Fractured surface of PCL/CNCs 4.0 wt% at 5000× magnification, **G** Lateral surface of PCL/CNCs 8.0 wt % at 30×, **H** Fractured surface of PCL/CNCs 8.0 wt% at 1000× magnification, and **I** Fractured surface of PCL/CNCs 8.0 wt% at 5000× magnification

content (Fig. 10G). The fracture surfaces (Fig. 10H, I) exhibited reduced deformation, indicating more brittle failure. Simultaneously, the number of cracks appearing on the fracture surface was higher than that on the fracture surface of the PCL/CNCs 4 wt % sample, which had the highest mechanical performance overall among the composites tested.

In-situ SEM micro tensile testing

Figure 11 shows the in situ analyses performed during the micro-tensile testing using SEM micrographs to gain insights into the morphology and failure of the specimens. The setup for the in situ tensile testing using a scanning electron microscope is shown in Fig. 11A. At a magnification of
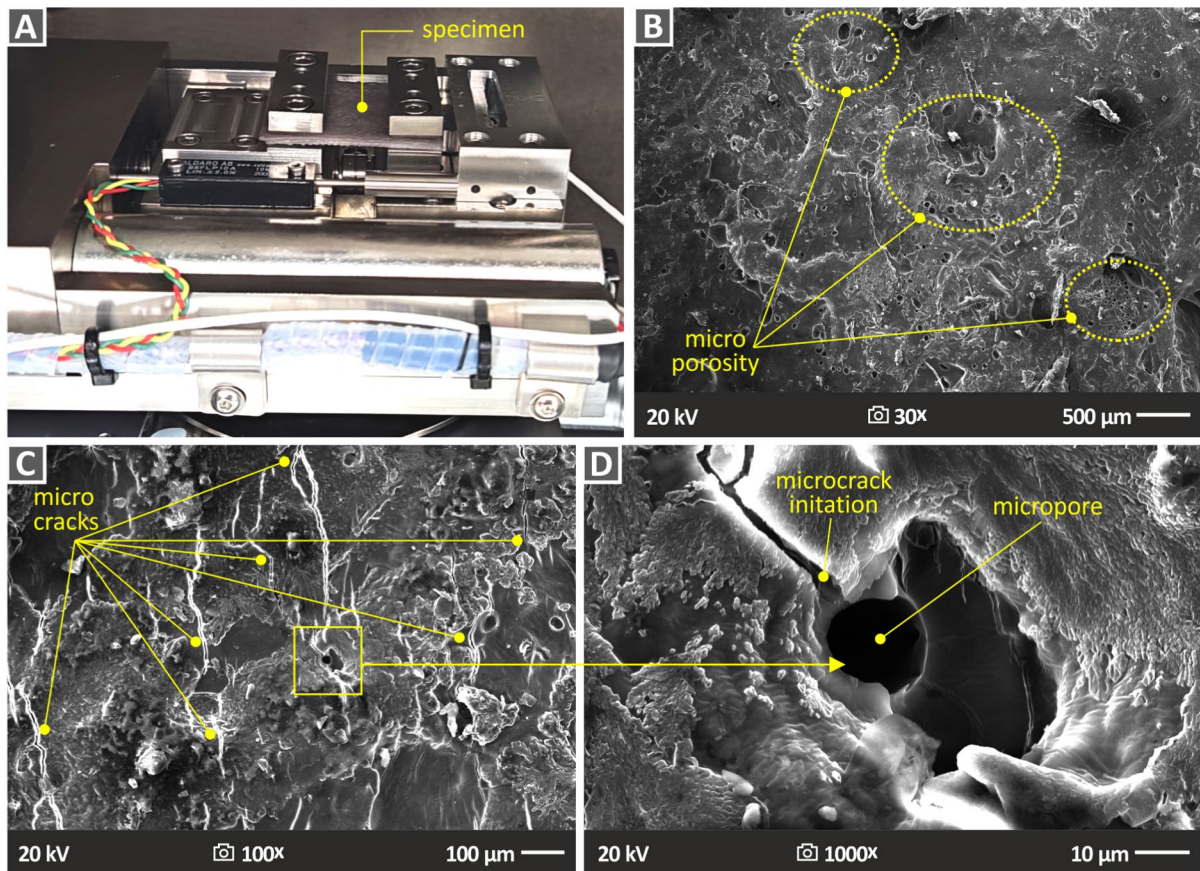
Fig. 11 **A** In situ micro-tensile testing setup **B** Surface microstructure of pure PCL in unloaded condition at 30×magnification, highlighting the presence of microporosity, **C** surface microstructure of pure PCL under 650 N loading at 100×magnification, highlighting the presence of microcracks, and **D** surface microstructure of pure PCL at 1000×magnification, highlighting micropore and microcrack initiation

30×, Fig. 11B shows the existence of micropores, where numerous voids can be observed when the specimen was in an unloaded condition. Figure 11C displays a specific region with microcracks generated owing to the applied tensile loading of 650 N at 100×magnification. A microcrack localized in the rim of a pore is shown at 1000×magnification in Fig. 11D. With this magnification, it is possible to examine the micropores and the region where the microcrack first appears more closely, providing a more thorough understanding of the crack initiation process, which appears to start from the pores in the structure of the sample. It should be noted that, in this test, only the pure PCL was tested, to reveal the mechanism and the response of the matrix material.

Micro-computed tomography investigations

Two distinct μ-CT scan specimens with nominal dimensions were fabricated, as shown in Fig. 3. The nominal over actual geometry comparison module (VG Studio MAX 2.2) was used to perform the dimensional deviation assessment in a color plot map form derived by comparing the CT voxel and CAD data. A comparison of the actual and nominal dimensions for typical experimental trials is shown in Fig. 12B and C. The color bar incorporated in the image demonstrates dimensional deviations in the range $-1500\ \mu m$ to $+1500\ \mu m$.

Additionally, in Fig. 12A, one diagram displays the estimated points' final variance distribution
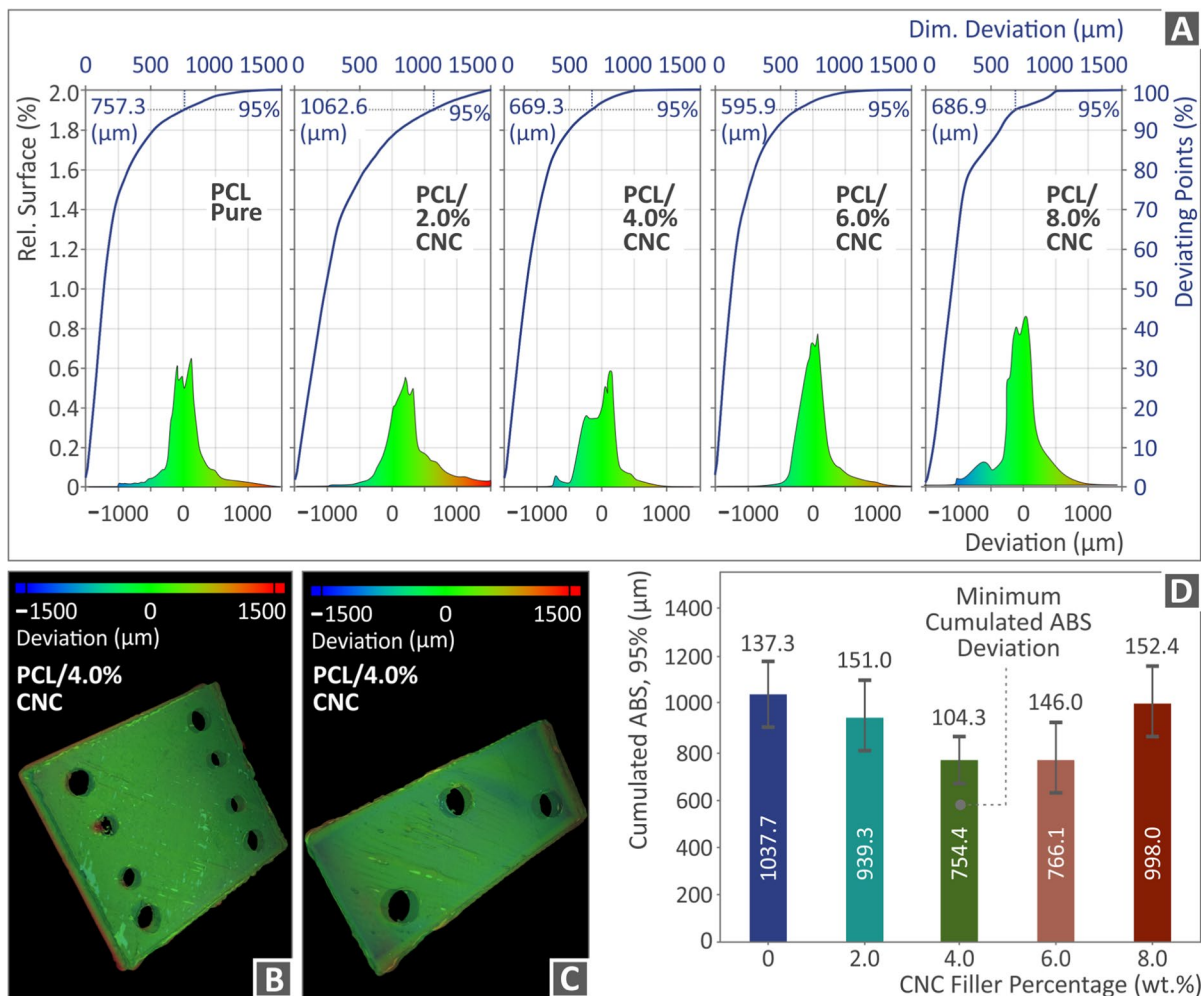
Fig. 12 Assessment of the dimensional accuracy (deviation from the nominal values) of the 3D-printed specimens based on actual to nominal comparison with the aid of CT voxel data. **A** Relative surface over-dimensional deviation and accumula-tive deviating points versus dimensional deviation. **B** and **C** Geometric deviations of the two types of μ-CT scan specimens with color-coded maps. **D** Chart of the minimum cumulative ABS (absolute) deviation for all fabricated bio-specimens

(in %) across the absolute dimensional deviation, whereas the other diagram presents a histogram that reveals the relative surface of the sample over the dimensional variation within the range of − 1000 μm to + 1000 μm. The same chart also shows the deviation, which is related to 95% of the measured points representing the difference between the actual and nominal specimen geometries. The test specimen, which contained 2.0 wt % CNCs showed a larger concentration of low positive deviations among all results. The specimens of 4 wt % CNCs exhibit the minimum values of absolute deviations, as shown in Fig. 12D.

Moreover, employing a sophisticated software tool (VGDefX v.2.2), the porosity assessment was carried out using the void analysis feature of the VG Studio MAX/2.2 software platform. This algorithm enables the detection of material voids and visualizes them in a color-coded plot. Quantitative data were obtained by determining multiple variables related to the dimensions, form, and position of the inbuilt voids. The two types of 3D CT-scanned specimens are shown in Fig. 13B and C, illustrating how the spatial dispersion of the voids reflects their volume, as indicated by the corresponding color scale. The relationships between void diameter, compactness, and sphericity
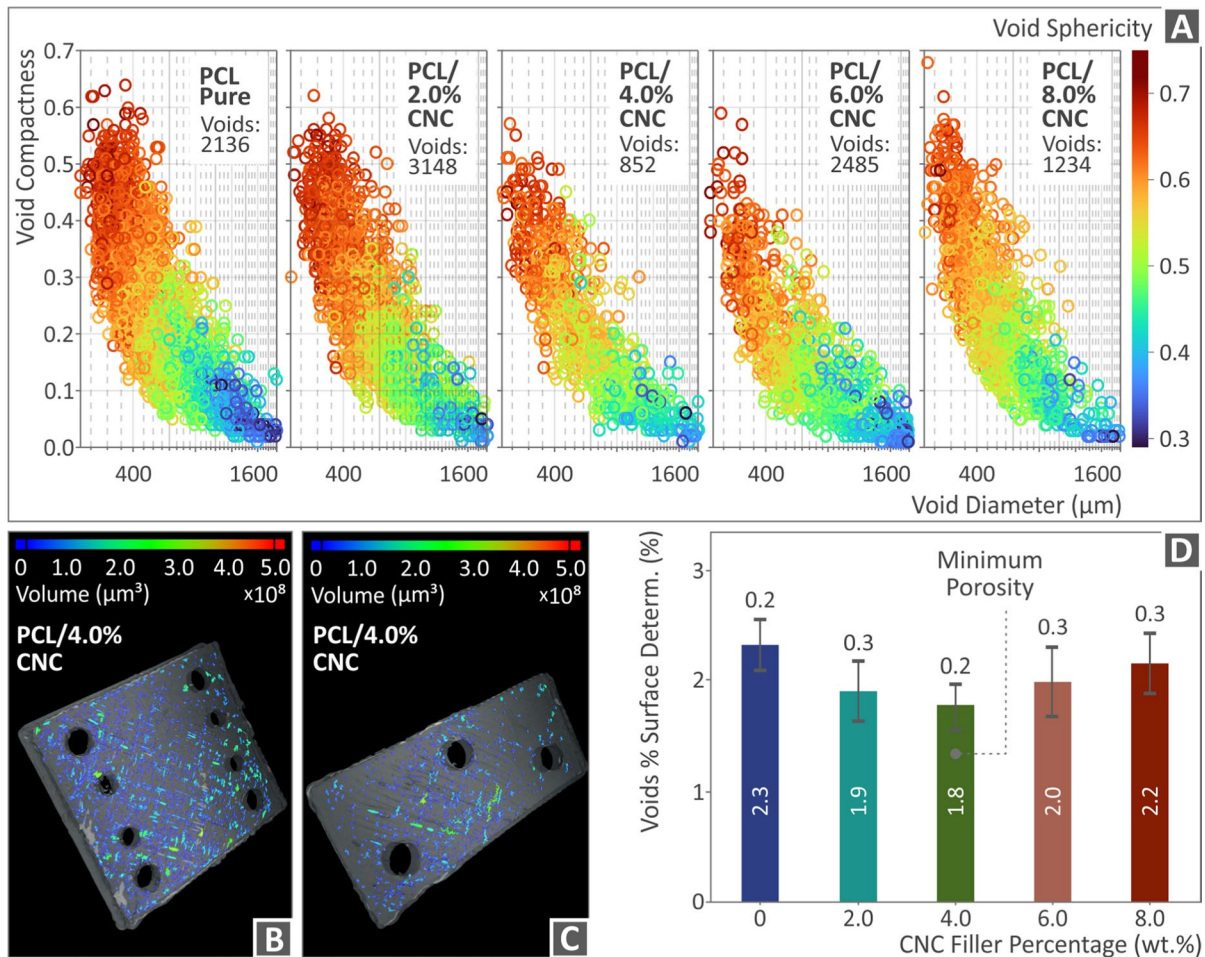
Fig. 13 A Void sphericity and void compactness over void diameter, **B** and **C** 3D color-coded map demonstrating the dispersion of voids with reference to the volume of the two types of μ-CT scan specimens, respectively, and **D** chart for the minimum porosity of all bio-specimens examined

are shown in Fig. 13A. The plot shows that most voids have spherical shapes and are small, indicating an elevated sphericity index. However, owing to their lack of compactness and tendency to extend parallel to the 3D printing strands, larger voids exhibit noticeably reduced sphericity. Finally, a specimen consisting of 4 wt % CNCs revealed the minimum porosity, as depicted in Fig. 13D. The pure PCL exhibited the highest porosity.

Discussion

The current study thoroughly examined the effects of incorporating CNCs into a PCL matrix in bio-plotting

3D printing. The incorporation of the CNCs enhanced the properties of the PCL matrix. Critical components that significantly influence the mechanical strength of composites are the interaction between the matrix and the additive and their influence on the rheological properties of the matrix. The incorporation of CNCs influenced the rheological properties of PCL. As the loading of CNCs in the nanocomposites increased, the viscosity also increased, up to 6 wt % load. The MFR increased to 4 wt % loaded composite.

In the Supplementary Material, Fig. A3 shows a spider chart for each of the three most significant metrics examined in this study: the tensile strength, MFR, and porosity. From the charts, the optimum response was achieved with the biocomposite of PCL/CNCs

4.0 wt %, displaying the maximum tensile strength, better MFR, and minimum porosity. In particular, the PCL/CNCs with 4 wt% percent samples showed the highest improvement in several of the mechanical properties assessed and showed high performance in the remaining mechanical properties related to tensile and flexural performance. The specific composite showed minimum absolute deviations from nominal to actual dimensional comparison, demonstrating that the enhancement in thermomechanical properties is directly related to the percentage of CNCs. Therefore, it can be stated that this loading is the most effective choice for the fabricated and tested bio compounds within the scope of this study. Because the composite (4 wt %) had the higher mechanical performance, the lowest porosity, and better dimensional accuracy, this indicates a possible connection between these qualities of the samples. The increase in the MFR is considered to be responsible for these outcomes, particularly considering that further increasing the CNCs loading reduces the MFR and increases the dimensional deviation and porosity. The reduced mechanical performance at concentrations greater than 4 wt % CNCs loading composites can be attributed to the additive starting to saturate on the nanocomposites. In this case, the increased MFR could not overcome the effect of filler saturation on the mechanical performance of the nanocomposites.

The saturation threshold of the CNCs nanoparticles was not assessed because it was beyond the scope of this study. The decrease in the mechanical performance of the 8 wt % nanocomposite can be attributed to this effect (Mostafa et al. 2020; Tamayo-Vegas et al. 2022). The saturation threshold is expected to occur at a higher filler loading because, even at the highest loading studied herein, the mechanical performance, although decreased, is still higher than that of the unfilled PCL polymer. The reinforcement of the PCL polymer by the addition of CNCs can be attributed to the reinforcement mechanism of the nanoparticles, which occurs because of the chemical interactions at the contact surface between the matrix and the nanoparticles and the restriction of the mobility of the polymeric chains up to a specific point, as described in the literature (Crosby and Lee 2007; Nguyen et al. 2016; Navarro Oliva et al. 2023).

Regarding the morphological characteristics, the fractured and lateral surfaces of the 3D bioprinted specimen microstructures were examined to comprehend the crucial aspects, including the layer thickness, fusion, interfaces between the layers, and general 3D bioprinting process quality. According to the SEM micrographs of the µ-CT scan specimens, micro-voids were found on the surface of the 3D bioprinted specimens during in situ micro-tensile testing. Furthermore, the presence of microcracks on the surface of the 3D bioprinted items was not exacerbated by the increase in filler concentration, as shown in the SEM micrographs of the lateral and fractured surfaces of the 3D bioprinted specimens. It is crucial to note that the samples did not have uniform layer morphologies and it was difficult to determine where the layers were connected. The microcracks in the vicinity of the pores on both the surface and internal microstructures of the specimens seem to initialize the failure of the sample. It should be noted that both the matrix (PCL) and filler (CNCs) are carbon-based materials; therefore, there is no safe way to distinguish the filler in the SEM images. However, carrying out EDS would not help for the same reason. Therefore, the dispersion of the filler in the matrix could not be evaluated using SEM and EDS. The process followed for the preparation of the composites and the low deviation between similar samples in the mechanical tests are indications of the good dispersion of the filler in the matrix. The high deviation values in the mechanical tests would suggest that the compositions of the samples differed.

SEM micro-tensile testing was performed solely on the pure PCL sample to understand the fracture mechanisms and their correlation with the 3D printed structure, specifically the inbuilt porosity. This objective was successfully achieved by examining the pure PCL sample, which showed that failure was initiated by the pores. Therefore, extending this type of investigation to composites is unnecessary. It can be reasonably assumed that reducing the number of pores can enhance the strength of a part. Further analysis of the µ-CT scan results demonstrated that an increase in the surface integrity of the samples positively affected their dimensional deviation. Notably, the sample with better dimensional accuracy exhibited a superior mechanical performance. This improvement can be attributed to the enhanced symmetry in the sample dimensions, which led to a more uniform stress distribution within the 3D-printed structure.

No similar nanocomposites have been documented in the existing literature concerning bioplotting 3D

printing utilizing either a similar or different methodology. A recent study used the same matrix material and CNFs as reinforcement and the samples were prepared with a similar method as the one followed herein. No significant differences were observed in the performance of the composites. For example, an improvement of approximately 20% in the tensile strength of the samples was observed (Vidakis et al. 2023c). Therefore, the use of CNCs or CNFs with a PCL matrix in bioplotting depends on the application, and the expected performance of the composite is similar. The effect of adding cellulose to the PCL matrix has been explored in previous studies, as mentioned in the relevant section of this work. In one study, an approximately 12% increase in mechanical properties was achieved (Alemán-Domínguez et al. 2018), whereas another study reported a reduction in flexural strength compared to pure PCL (Lee et al. 2011; Alemán-Domínguez et al. 2019). In the context of MEX 3D printing, incorporating cellulose into the polycarbonate matrix resulted in an approximately 10% increase in the mechanical strength (Vidakis et al. 2021), and a similar effect was observed for the polylactic acid polymer (Petousis et al. 2022). In a polyamide matrix, a much higher improvement of 24% in tensile strength was reported (Vidakis et al. 2023f). When cellulose was used as a reinforcement in resins for VPP 3D printing, an impressive increase of over 100% in the tensile strength was reported (Vidakis et al. 2022a). These variations in the results can be attributed to differences in the preparation processes and initial states of the raw materials, particularly considering that VPP 3D printing involves raw liquid materials.

Compared to the aforementioned studies using different processes and applications, the addition of CNCs to the PCL matrix, following the process presented in this research for bio-plotting 3D printing, exhibited a more favorable reinforcement effect. The PCL/CNCs compounds demonstrated greater mechanical improvements than the PCL/cellulose composites reported thus far, even those prepared using different processes and intended for various applications. Similarly, in MEX 3D printing, where a similar thermomechanical process (extrusion) was utilized to prepare filaments, the PCL/CNCs nanocomposites presented here displayed better mechanical performance than those in the corresponding studies on MEX 3D printing mentioned above. The disparity in the reinforcement effect can be attributed, among other factors, to the differences in the 3D printing processes used, including the unique characteristics of bioplotting and the different raw material grades.

The inclusion of CNCs particles in medical-grade PCL matrices has delivered promising results for the fabrication of biocompatible and bioabsorbable composites. The thermomechanical properties of the PCL-based materials were significantly enhanced as a result of this addition. The mechanical properties of the composites increased in terms of the tensile strength, flexural strength, stiffness, and rheological properties, demonstrating higher MFR values. Additionally, it has been shown that employing CNCs as a reinforcement agent enhances the overall performance of biocomposite materials because they exhibit minimal variance between nominal and actual dimensions and minimal porosity, opening up opportunities for additional biomedical applications where these characteristics are desirable.

Conclusions

In this study, 3D bioprinted specimens were created using a 3D bioprinting process, providing a robust analysis of the reinforcement mechanisms by incorporating CNCs particles into a biocompatible medical-grade PCL matrix material. An industrial-scale 3D bio-plotter was used to manufacture four different types of specimens (designed for tensile, flexural, and in situ micro-tensile testing) made from PCL/CNCs filaments to ascertain how CNCs as fillers affect their thermomechanical and rheological properties, in combination with a morphological examination employing SEM and AFM. Fourteen different experiments were performed to determine the effect of the CNCs addition on the overall performance of the materials. The prepared nanocomposites were fully characterized, and the experimental findings were analyzed and correlated to thoroughly understand the effects and mechanisms triggered by adding CNCs to the PCL matrix. The key findings of this study are summarized as follows:

- All the biocomposites produced showed some improvement in performance.

- In this study, a biocomposite containing 4 wt % CNCs demonstrated the most noticeable improvement in all tests carried out in the present research.
- It also showed enhanced MFR, suggesting superior flowability throughout the production process.
- It exhibited lower porosity, resulting in a denser and stiffer structure.
- It can be concluded that these properties are correlated and affect each other in terms of the overall performance of the composites.
- The fabrication was exact and consistent, as evidenced by the minimal variation in the specified parameters in terms of dimensional accuracy.

A biocomposite with a 4 wt % CNCs proved to be particularly useful for a variety of applications, as it offers increased stiffness compared to pure PCL and contains favorable attributes such as improved flowability, reduced porosity, and dimensional precision. By enhancing the mechanical performance of the PCL in this way, a scaffold-ready nanocomposite is available, capable of sustaining higher stresses than the unfilled polymer. In future research, different biocompatible additives will be evaluated for their reinforcing effects on the PCL polymer in bioplotting.

Declarations

References

Alemán-Domínguez ME, Giusto E, Ortega Z, Tamaddon M, Benítez AN, Liu C (2019) Three-dimensional printed polycaprolactone-microcrystalline cellulose scaffolds. J Biomed Mater Res B Appl Biomater 107:521–528. https://doi.org/10.1002/jbm.b.34142

Alemán-Domínguez ME, Ortega Z, Benítez AN, Monzón M, Garzón LV, Ajami S, Liu C (2018) Polycaprolactone–carboxymethyl cellulose composites for manufacturing porous scaffolds by material extrusion. Biodes Manuf 1:245–253. https://doi.org/10.1007/s42242-018-0024-z

Arif ZU, Khalid MY, Noroozi R, Hossain M, Shi HH, Tariq A, Ramakrishna S, Umer R (2023) Additive manufacturing of sustainable biomaterials for biomedical applications. Asian J Pharm Sci 18:100812. https://doi.org/10.1016/j.ajps.2023.100812

Arif ZU, Khalid MY, Noroozi R, Sadeghianmaryan A, Jalalvand M, Hossain M (2022) Recent advances in 3D-printed polylactide and polycaprolactone-based biomaterials for tissue engineering applications. Int J Biol Macromol 218:930–968. https://doi.org/10.1016/j.ijbiomac.2022.07.140

Avella A, Idström A, Mincheva R, Nakayama K, Evenäs L, Raquez J-M, Lo Re G (2022) Reactive melt crosslinking of cellulose nanocrystals/poly (ε-caprolactone) for heat-shrinkable network. Compos Part A Appl Sci Manuf 163:107166. https://doi.org/10.1016/j.compositesa.2022.107166

Baranov A, Sommerhoff F, Curnow OJ, Staiger MP (2023) Prospects for manufacturing of complex 3D-shaped all-cellulose composites. Compos Part A Appl Sci Manuf 173:107627. https://doi.org/10.1016/j.compositesa.2023.107627

Bauer AJP, Wu Y, Li B (2016) Electrospun poly (ε-caprolactone)/polyhedral oligomeric

silsesquioxane-based copolymer blends: evolution of fiber internal structures. Macromol Biosci 16:705–716. https://doi.org/10.1002/mabi.201500399

Beaugrand J, Berzin F (2013) Lignocellulosic fiber reinforced composites: influence of compounding conditions on defibrization and mechanical properties. J Appl Polym Sci 128:1227–1238. https://doi.org/10.1002/app.38468

Billiet T, Vandenhaute M, Schelfhout J, Van Vlierberghe S, Dubruel P (2012) A review of trends and limitations in hydrogel-rapid prototyping for tissue engineering. Biomaterials 33:6020–6041. https://doi.org/10.1016/j.biomaterials.2012.04.050

Camerlingo C, Zenone F, Delfino I, Diano N, Mita DG, Lepore M (2007) Investigation on clarified fruit juice composition by using visible light micro-raman spectroscopy. Sensors 7:2049–2061. https://doi.org/10.3390/s7102049

Chylińska M, Szymańska-Chargot M, Zdunek A (2014) Imaging of polysaccharides in the tomato cell wall with Raman microspectroscopy. Plant Methods 10:14. https://doi.org/10.1186/1746-4811-10-14

Crosby AJ, Lee J (2007) Polymer nanocomposites: the "nano" effect on mechanical properties. Polym Rev 47:217–229. https://doi.org/10.1080/15583720701271278

Du H, Liu W, Zhang M, Si C, Zhang X, Li B (2019) Cellulose nanocrystal and cellulose nanofibrils based hydrogels for biomedical applications. Carbohydr Polym 209:130–144. https://doi.org/10.1016/j.carbpol.2019.01.020

El-hadi AM (2017) Increase the elongation at break of poly (lactic acid) composites for use in food packaging films. Sci Rep 7:46767. https://doi.org/10.1038/srep46767

Gatin E, Iordache S-M, Matei E, Luculescu C-R, Iordache A-M, Grigorescu CEA, Ilici RR (2022) Raman spectroscopy as spectral tool for assessing the degree of conversion after curing of two resin-based materials used in restorative dentistry. Diagnostics. https://doi.org/10.3390/diagnostics12081993

Ghorbani FM, Kaffashi B, Shokrollahi P, Seyedjafari E, Ardeshirylajimi A (2015) PCL/chitosan/Zn-doped nHA electrospun nanocomposite scaffold promotes adipose derived stem cells adhesion and proliferation. Carbohydr Polym 118:133–142. https://doi.org/10.1016/j.carbpol.2014.10.071

Giraud M-N, Guex AG, Tevaearai HT (2012) Cell therapies for heart function recovery: focus on myocardial tissue engineering and nanotechnologies. Cardiol Res Pract 2012:971614. https://doi.org/10.1155/2012/971614

Gong J, Li J, Xu J, Xiang Z, Mo L (2017) Research on cellulose nanocrystal produced from cellulose sources with various polymorphs. RSC Adv 7:33486–33493. https://doi.org/10.1039/C7RA06222B

Grenier J, Duval H, Barou F, Lv P, David B, Letourneur D (2019) Mechanisms of pore formation in hydrogel scaffolds textured by freeze-drying. Acta Biomater 94:195–203. https://doi.org/10.1016/j.actbio.2019.05.070

Grishkewich N, Mohammed N, Tang J, Tam KC (2017) Recent advances in the application of cellulose nanocrystal. Curr Opin Colloid Interface Sci 29:32–45. https://doi.org/10.1016/j.cocis.2017.01.005

binti HashimH, binti EmranNAA, Isono T, Katsuhara S, Ninoyu H, Matsushima T, Yamamoto T, Borsali R, Satoh T, Tajima K (2022) Improving the mechanical properties of polycaprolactone using functionalized nanofibrillated bacterial cellulose with high dispersibility and long fiber length as a reinforcement material. Compos Part A Appl Sci Manuf 158:106978. https://doi.org/10.1016/j.compositesa.2022.106978

Binti HashimH, Binti EmranNAA, Isono T, Katsuhara S, Ninoyu H, Matsushima T, Yamamoto T, Borsali R, Satoh T, Tajima K (2022) Improving the mechanical properties of polycaprolactone using functionalized nanofibrillated bacterial cellulose with high dispersibility and long fiber length as a reinforcement material. Compos Part A Appl Sci Manuf 158:106978. https://doi.org/10.1016/j.compositesa.2022.106978

Hausmann MK, Rühs PA, Siqueira G, Läuger J, Libanori R, Zimmermann T, Studart AR (2018) Dynamics of cellulose nanocrystal alignment during 3D printing. ACS Nano 12:6926–6937. https://doi.org/10.1021/acsnano.8b02366

He X, Lu Q (2023) Design and fabrication strategies of cellulose nanocrystal-based hydrogel and its highlighted application using 3D printing: A review. Carbohydr Polym 301:120351. https://doi.org/10.1016/j.carbpol.2022.120351

Hutmacher DW (2000) Scaffolds in tissue engineering bone and cartilage. Biomaterials 21:2529–2543

Jian H, Wang M, Wang S, Wang A, Bai S (2018) 3D bioplotting for cell culture and tissue fabrication. Biodes Manuf 1:45–61. https://doi.org/10.1007/s42242-018-0006-1

Kačarević ŽP, Rider PM, Alkildani S, Retnasingh S, Smeets R, Jung O, Ivanišević Z, Barbeck M (2018) An introduction to 3D bioplotting: possibilities. Chall Future Asp Mater 11(11):2199

Khalid MY, Al Rashid A, Arif ZU, Ahmed W, Arshad H (2021) Recent advances in nanocellulose-based different biomaterials: types, properties, and emerging applications. J Mater Res Technol 14:2601–2623. https://doi.org/10.1016/j.jmrt.2021.07.128

Khalid MY, Arif ZU, Noroozi R, Hossain M, Ramakrishna S, Umer R (2023) 3D/4D printing of cellulose nanocrystals-based biomaterials: Additives for sustainable applications. Int J Biol Macromol 251:126287. https://doi.org/10.1016/j.ijbiomac.2023.126287

Kholgh Eshkalak S, Rezvani Ghomi E, Dai Y, Choudhury D, Ramakrishna S (2020) The role of three-dimensional printing in healthcare and medicine. Mater Des 194:108940. https://doi.org/10.1016/j.matdes.2020.108940

Lam E, Male KB, Chong JH, Leung ACW, Luong JHT (2012) Applications of functionalized and nanoparticle-modified nanocrystalline cellulose. Trends Biotechnol 30:283–290. https://doi.org/10.1016/j.tibtech.2012.02.001

Lee SH, Teramoto Y, Endo T (2011) Cellulose nanofiber-reinforced polycaprolactone/polypropylene hybrid nanocomposite. Compos Part A Appl Sci Manuf 42:151–156. https://doi.org/10.1016/j.compositesa.2010.10.014

Li VC-F, Kuang X, Hamel CM, Roach D, Deng Y, Qi HJ (2019) Cellulose nanocrystal support material for 3D printing complexly shaped structures via multi-materials-multi-methods printing. Addit Manuf 28:14–22. https://doi.org/10.1016/j.addma.2019.04.013

Li VC-F, Kuang X, Mulyadi A, Hamel CM, Deng Y, Qi HJ (2019b) 3D printed cellulose nanocrystal composites

through digital light processing. Cellulose 26:3973–3985. https://doi.org/10.1007/s10570-019-02353-9

Liao G-Y, Zhou X-P, Chen L, Zeng X-Y, Xie X-L, Mai Y-W (2012) Electrospun aligned PLLA/PCL/functionalised multiwalled carbon nanotube composite fibrous membranes and their bio/mechanical properties. Compos Sci Technol 72:248–255. https://doi.org/10.1016/j.compscitech.2011.11.009

Lin Z, Guo X, He Z, Liang X, Wang M, Jin G (2021) Thermal degradation kinetics study of molten polylactide based on Raman spectroscopy. Polym Eng Sci 61:201–210. https://doi.org/10.1002/pen.25568

Liu X, Zou Y, Li W, Cao G, Chen W (2006) Kinetics of thermo-oxidative and thermal degradation of poly (d, l-lactide) (PDLLA) at processing temperature. Polym Degrad Stab 91:3259–3265. https://doi.org/10.1016/j.polymdegradstab.2006.07.004

Luiz BKM, Amboni RDMC, Prates LHM, Roberto Bertolino J, Pires ATN (2007) Influence of drinks on resin composite: Evaluation of degree of cure and color change parameters. Polym Test 26:438–444. https://doi.org/10.1016/j.polymertesting.2006.12.005

Ma T, Lv L, Ouyang C, Hu X, Liao X, Song Y, Hu X (2021) Rheological behavior and particle alignment of cellulose nanocrystal and its composite hydrogels during 3D printing. Carbohydr Polym 253:117217. https://doi.org/10.1016/j.carbpol.2020.117217

Makarem M, Lee CM, Kafle K, Huang S, Chae I, Yang H, Kubicki JD, Kim SH (2019) Probing cellulose structures with vibrational spectroscopy. Cellulose 26:35–79. https://doi.org/10.1007/s10570-018-2199-z

Mazzanti V, Malagutti L, Mollica F (2019) FDM 3D printing of polymers containing natural fillers: a review of their mechanical properties. Polymers (Basel). https://doi.org/10.3390/polym11071094

Mironov V, Reis N, Derby B (2006) Review: bioplotting: a beginning. Tissue Eng 12:631–634. https://doi.org/10.1089/ten.2006.12.631

Moon RJ, Martini A, Nairn J, Simonsen J, Youngblood J (2011) Cellulose nanomaterials review: structure, properties and nanocomposites. Chem Soc Rev 40:3941–3994. https://doi.org/10.1039/C0CS00108B

Mostafa SA, Faried AS, Farghali AA, EL-Deeb MM, Tawfik TA, Majer S, Abd Elrahman M (2020) Influence of nanoparticles from waste materials on mechanical properties. Durab Microstruct UHPC Mater 13(20):4530

Mujtaba M, Salaberria AM, Andres MA, Kaya M, Gunyakti A, Labidi J (2017) Utilization of flax (Linum usitatissimum) cellulose nanocrystal as reinforcing material for chitosan films. Int J Biol Macromol 104:944–952

Navarro Oliva FS, Sahihi M, Lenglet L, Ospina A, Guenin E, Jaramillo-Botero A, Goddard WA, Bedoui F (2023) Nanoparticle size and surface chemistry effects on mechanical and physical properties of nano-reinforced polymers: The case of PVDF-Fe3O4 nano-composites. Polym Test 117:107851. https://doi.org/10.1016/j.polymertesting.2022.107851

Nguyen TA, Nguyen TH, Nguyen TV, Thai H, Shi Xianming (2016) Effect of nanoparticles on the thermal and mechanical properties of epoxy coatings. J Nanosci Nanotechnol 16(9):9874–9881

Noguchi T, Bamba Y, Odaka I, Iwamoto R, Endo M, Isogai A (2023) Natural rubber composites with high strength, modulus, water-resistance, and thermal stability, prepared with cellulose nanofibrils and sodium methacrylate. Compos Part A Appl Sci Manuf 173:107665. https://doi.org/10.1016/j.compositesa.2023.107665

Nonato RC, Mei LHI, Bonse BC, Chinaglia EF, Morales AR (2019) Nanocomposites of PLA containing ZnO nanofibers made by solvent cast 3D printing: Production and characterization. Eur Polym J 114:271–278. https://doi.org/10.1016/j.eurpolymj.2019.02.026

Ozbolat IT, Peng W, Ozbolat V (2016) Application areas of 3D bioplotting. Drug Discov Today 21:1257–1271. https://doi.org/10.1016/j.drudis.2016.04.006

Palaganas NB, Mangadlao JD, de Leon ACC, Palaganas JO, Pangilinan KD, Lee YJ, Advincula RC (2017) 3D printing of photocurable cellulose nanocrystal composite for fabrication of complex architectures via stereolithography. ACS Appl Mater Interfaces 9:34314–34324. https://doi.org/10.1021/acsami.7b09223

Peltola SM, Melchels FPW, Grijpma DW, Kellomäki M (2008) A review of rapid prototyping techniques for tissue engineering purposes. Ann Med 40:268–280. https://doi.org/10.1080/07853890701881788

Peris-Díaz M, Łydżba-Kopczyńska B, Sentandreu E (2018) Raman spectroscopy coupled to chemometrics to discriminate provenance and geological age of amber. J Raman Spectrosc. https://doi.org/10.1002/jrs.5357

Petousis M, Vidakis N, Mountakis N, Papadakis V, Kanellopoulou S, Gaganatsiou A, Stefanoudakis N, Kechagias J (2022) Multifunctional material extrusion 3D-printed antibacterial polylactic acid (PLA) with binary inclusions: the effect of cuprous oxide and cellulose nanofibers. Fibers. https://doi.org/10.3390/fib10060052

Place ES, Evans ND, Stevens MM (2009) Complexity in biomaterials for tissue engineering. Nat Mater 8:457–470. https://doi.org/10.1038/nmat2441

Prasad A, Sankar MR, Katiyar V (2017) State of Art on Solvent Casting Particulate Leaching Method for Orthopedic ScaffoldsFabrication. Mater Today Proc 4:898–907. https://doi.org/10.1016/j.matpr.2017.01.101

Qiu C, Zhu K, Zhou X, Luo L, Zeng J, Huang R, Lu A, Liu X, Chen F, Zhang L, Fu Q (2018) Influences of coagulation conditions on the structure and properties of regenerated cellulose filaments via wet-spinning in LiOH/urea solvent. ACS Sustain Chem Eng 6:4056–4067. https://doi.org/10.1021/acssuschemeng.7b04429

Scaffaro R, Lopresti F, Botta L, Rigogliuso S, Ghersi G (2016) Melt processed PCL/PEG scaffold with discrete pore size gradient for selective cellular infiltration. Macromol Mater Eng 301:182–190

Scaffaro R, Lopresti F, Maio A, Botta L, Rigogliuso S, Ghersi G (2017) Electrospun PCL/GO-g-PEG structures: Processing-morphology-properties relationships. Compos Part A Appl Sci Manuf 92:97–107. https://doi.org/10.1016/j.compositesa.2016.11.005

Scaffaro R, Lopresti F, Sutera A, Botta L, Fontana RM, Puglia AM, Gallo G (2016) Effect of PCL/PEG-Based Membranes on Actinorhodin Production in Streptomyces coelicolor Cultivations. Macromol Biosci 16:686–693. https://doi.org/10.1002/mabi.201500391

Seol Y-J, Kang H-W, Lee SJ, Atala A, Yoo JJ (2014) Bioplotting technology and its applications. Eur J Cardiothorac Surg 46:342–348. https://doi.org/10.1093/ejcts/ezu148

Seol Y-J, Kang T-Y, Cho D-W (2012) Solid freeform fabrication technology applied to tissue engineering with various biomaterials. Soft Matter 8:1730–1735. https://doi.org/10.1039/C1SM06863F

Simonini L, Mahmood H, Dorigato A, Pegoretti A (2023) Evaluation of self-healing capability of a polycaprolactone interphase in epoxy/glass composites. Compos Part A Appl Sci Manuf 169:107539. https://doi.org/10.1016/j.compositesa.2023.107539

Stuart BH (1996) Temperature studies of polycarbonate using Fourier transform Raman spectroscopy. Polym Bull 36:341–346. https://doi.org/10.1007/BF00319235

Tamayo-Vegas S, Muhsan A, Liu C, Tarfaoui M, Lafdi K (2022) The effect of agglomeration on the electrical and mechanical properties of polymer matrix nanocomposites reinforced with carbon nanotubes. Polymers (Basel) 14(9):1842

Tariq A, Arif ZU, Khalid MY, Hossain M, Rasool PI, Umer R, Ramakrishna S (2023) Recent Advances in the Additive Manufacturing of Stimuli-Responsive Soft Polymers. Adv Eng Mater 25:2301074. https://doi.org/10.1002/adem.202301074

Vidakis N, Kalderis D, Petousis M, Maravelakis E, Mountakis N, Bolanakis N, Papadakis V (2023a) Biochar filler in MEX and VPP additive manufacturing: characterization and reinforcement effects in polylactic acid and standard grade resin matrices. Biochar 5:39. https://doi.org/10.1007/s42773-023-00238-6

Vidakis N, Petousis M, David CN, Sagris D, Mountakis N (2023) Biomedical resin reinforced with Cellulose Nanofibers (CNF) in VAT photopolymerization (VPP) Additive Manufacturing (AM): The effect of filler loading and process control parameters on Critical Quality Indicators (CQIs). J Manuf Process 101:755–769. https://doi.org/10.1016/j.jmapro.2023.06.018

Vidakis N, Petousis M, Michailidis N, David C, Mountakis N, Papadakis V, Sfakiotakis E, Sagris D, Spiridaki M, Argyros A (2023) Optimized PCL/CNF bio-nanocomposites for medical bio-plotted applications: rheological, structural, and thermomechanical aspects. Bioplotting. https://doi.org/10.1016/j.bprint.2023.e00311

Vidakis N, Petousis M, Michailidis N, Kechagias JD, Mountakis N, Argyros A, Boura O, Grammatikos S (2022a) High-performance medical-grade resin radically reinforced with cellulose nanofibers for 3D printing. J Mech Behav Biomed Mater 134:105408. https://doi.org/10.1016/j.jmbbm.2022.105408

Vidakis N, Petousis M, Michailidis N, Mountakis N, Papadakis V, Argyros A, Charou C (2023) Polyethylene glycol and polyvinylpyrrolidone reduction agents for medical grade polyamide 12/silver nanocomposites development for material extrusion 3D printing: Rheological, thermomechanical, and biocidal performance. React Funct Polym. https://doi.org/10.1016/j.reactfunctpolym.2023.105623

Vidakis N, Petousis M, Michailidis N, Mountakis N, Papadakis V, Argyros A, Charou C (2023e) Medical grade polyamide 12 silver nanoparticle filaments fabricated with in-situ reactive reduction melt-extrusion: rheological, thermomechanical, and bactericidal performance in MEX 3D printing. Appl Nanosci. https://doi.org/10.1007/s13204-023-02966-4

Vidakis N, Petousis M, Michailidis N, Papadakis V, Korlos A, Mountakis N, Argyros A (2022b) Multi-Functional 3D-Printed Vat Photopolymerization Biomedical-Grade Resin Reinforced with Binary Nano Inclusions: The Effect of Cellulose Nanofibers and Antimicrobial Nanoparticle Agents. Polymers (basel) 14:1–24. https://doi.org/10.3390/polym14091903

Vidakis N, Petousis M, Mountakis N, Grammatikos S, Papadakis V, Kechagias JD, Das SC (2022) On the thermal and mechanical performance of Polycarbonate / Titanium Nitride nanocomposites in material extrusion additive manufacturing. Compos C Op Access. https://doi.org/10.1016/j.jcomc.2022.100291

Vidakis N, Petousis M, Mountakis N, Papadakis V, Moutsopoulou A (2023f) Mechanical strength predictability of full factorial, Taguchi, and Box Behnken designs: Optimization of thermal settings and Cellulose Nanofibers content in PA12 for MEX AM. J Mech Behav Biomed Mater 142:105846. https://doi.org/10.1016/j.jmbbm.2023.105846

Vidakis N, Petousis M, Moutsopoulou A, Mountakis N, Grammatikos S, Papadakis V, Tsikritzis D (2023g) Biomedical Engineering Advances Cost-effective bi-functional resin reinforced with a nano-inclusion blend for vat photopolymerization additive manufacturing : The effect of multiple antibacterial nanoparticle agents. Biomed Eng Adv 5:100091. https://doi.org/10.1016/j.bea.2023.100091

Vidakis N, Petousis M, Velidakis E, Mountakis N, Grammatikos SA, Tzounis L (2023) Multi-functional medical grade Polyamide12/Carbon Black nanocomposites in material extrusion 3D printing. Compos Struct. https://doi.org/10.1016/j.compstruct.2023.116788

Vidakis N, Petousis M, Velidakis E, Spiridaki M, Kechagias JD (2021) Mechanical performance of fused filament fabricated and 3d-printed polycarbonate polymer and polycarbonate/ cellulose nanofiber nanocomposites. Fibers 9:74. https://doi.org/10.3390/fib9110074

Wang J, Chiappone A, Roppolo I, Shao F, Fantino E, Lorusso M, Rentsch D, Dietliker K, Pirri CF, Grützmacher H (2018) All-in-One Cellulose Nanocrystal for 3D Printing of Nanocomposite Hydrogels. Angew Chem Int Ed 57:2353–2356. https://doi.org/10.1002/anie.201710951

Yu B, Zhao Z, Fu S, Meng L, Liu Y, Chen F, Wang K, Fu Q (2019) Fabrication of PLA/CNC/CNT conductive composites for high electromagnetic interference shielding based on Pickering emulsions method. Compos Part A Appl Sci Manuf. https://doi.org/10.1016/j.compositesa.2019.105558

Zhang C, Wang L, Zhai T, Wang X, Dan Y, Turng L-S (2016) The surface grafting of graphene oxide with poly (ethylene glycol) as a reinforcement for poly (lactic acid) nanocomposite scaffolds for potential tissue engineering applications. J Mech Behav Biomed Mater. https://doi.org/10.1016/j.jmbbm.2015.08.043

Zhang S, Liu J, Guo Q, Wei N, Ning Y, Bai Y, Tian Y, Wang T, Sun Z, Pu Y (2023) Fabrication of cellulose-based dielectric nanocomposite film with excellent energy storage performance via codissolution-regeneration method. Compos Part A Appl Sci Manuf. https://doi.org/10.1016/j.compositesa.2022.107329

Zhu W, Masood F, O'Brien J, Zhang LG (2015) Highly aligned nanocomposite scaffolds by electrospinning and

electrospraying for neural tissue regeneration. Nanomedicine. https://doi.org/10.1016/j.nano.2014.12.001

Zimmerer C, Matulaitiene I, Niaura G, Reuter U, Janke A, Boldt R, Sablinskas V, Steiner G (2019) Nondestructive characterization of the polycarbonate - octadecylamine interface by surface enhanced Raman spectroscopy. Polym Test. https://doi.org/10.1016/j.polymertesting.2018.11.023ss